

Copyright
by
Michael Goegler
2002

Light-induced Actin Polymerization *in vitro* and *in vivo*

by

Michael Goegler,

THESIS

Presented to the Faculty of the Graduate School of

The University of Texas at Austin

in Partial Fulfillment

of the Requirements

for the Degree of

MASTER OF ARTS

THE UNIVERSITY OF TEXAS AT AUSTIN

August 2002

Light-induced Actin Polymerization *in vitro* and *in vivo*

APPROVED BY

SUPERVISING COMMITTEE:

Mark Raizen, Supervisor

Josef Käs

Für meine Eltern und meine Schwester

Acknowledgments

I want to thank Prof. Mark Raizen for giving me the opportunity to work in his research group. Mark is full of ideas and I did learn a lot in this year. I also appreciated his attitude to teach in the lab and to work there together with his students. I had a lot of fun.

I also want to acknowledge Prof. Josef Käs for the close collaboration with his lab. His funded knowledge in biology and the resultant suggestions were very helpful. I received much support from him.

I felt as an appendant group member in both laboratories. The atmosphere was friendly and relaxed, and people were willing to help with problems. Therefore, my stay was very pleasant and I did learn very much.

Thanks to Allen Ehrlicher, who worked with me on the cell motility part, for all your help. Also thanks to Björn Stuhmann, Daniel Koch, and Timo Betz who affiliated me very nicely as a member of the BONG-group.

I would like to acknowledge Windell Oskay, alias Dr. Who, and Todd Meyrath, who helped me with editing this document. Windell, thanks for providing me with the excellent coffee during the whole year. Thanks also goes to the other members of the Raizen group: Artëm Dudarev, Braulio Gutiérrez, Chih-sung Chuu, Chuanwei Zhang, Florian Schreck, Greg Henry, Jay Hansson, Joshua Elliot, Kevin Henderson, Robert Morgan, and Samantha Moore. It was really nice working with you.

Also, I want to acknowledge the other members of the Käs group: Ann Marie Navar, Bryan Lincoln, Brian Gentry, Chieze Ibeneche, Douglas Martin, David Humphrey, David Smith, Falk Wottawah, Jochen Guck, Martin Forstner, Revathi Ananthakrishnan, Stefan Schinkinger, and Vanessa Bell. I had a good time with you.

Thanks to Jack in the machine shop for all the patience with me. Basically everything I know about machining I learnt from you.

I would like to acknowledge my family and my friends, who endorsed me very much.

Michael Goegler

The University of Texas at Austin

August 2002

Light-induced Actin Polymerization *in vitro* and *in vivo*

Michael Goegler, M.A.

The University of Texas at Austin, 2002

Supervisor: Mark Raizen

This work describes experiments on light-induced actin polymerization *in vitro* as well as *in vivo*. Therefore, a laser beam is used to produce a dipole force on the polarizable sample, in this case actin. Due to this force, actin monomers and oligomers drift into the center of the laser spot. This results in a concentration increment of actin in the laser spot.

After a brief introduction to polymerization of actin *in vitro*, the experimental setup and procedures will be presented, followed by a theoretical approach, used to determine the concentration enhancement and the strength of the dipole force. A short discussion of the obtained results will be given.

In vivo, experiments were done on fibroblasts and fish epidermal keratocytes. A general introduction to cell structure and cell motility will be presented. Experimental procedures for both cell types will be shown. Results of the “optical cell guiding” experiments and further directions will be discussed.

Table of Contents

Acknowledgments	v
Abstract	vii
List of Tables	xi
List of Figures	xii
Chapter 1. Introduction	1
Part I Light-induced Actin Polymerization	4
Chapter 2. About Actin	5
2.1 General Information about Actin	5
2.2 Actin Monomers	6
2.3 Structure of F-Actin	7
2.4 Kinetics of Polymerization	9
2.4.1 Nucleation and Elongation	9
2.4.2 Time Evolution of Actin Polymerization	10
2.4.3 ATP- and ADP-Actin Assembly	12
2.4.4 Influences on Actin Polymerization	13
Chapter 3. <i>In vitro</i> Experiment	16
3.1 Light-induced Actin Polymerization	16
3.2 Experimental Procedure	17
3.2.1 Preparation of Sample	17
3.2.2 Fluorescence Microscopy	19
3.2.3 Cooling of Sample	21
3.3 Experimental Setup	23

Chapter 4. Theoretical Approach to Actin Polymerization	28
4.1 Polarizability of Actin	28
4.1.1 Refractive Index of G-actin	28
4.1.2 Polarizability	29
4.2 Dipole Force	30
4.3 Concentration Enhancement	33
Chapter 5. Conclusion and Outlook	36
Part II Optical Cell Guiding	38
Chapter 6. The Cytoskeleton of a Cell	39
6.1 Microfilaments	40
6.1.1 The Actin Cytoskeleton	40
6.1.2 Actin Sequestering Proteins	42
6.1.3 Capping and Severing Proteins	43
6.1.4 Myosin	44
6.2 Microtubules	46
6.2.1 Composition and Assembly	46
6.2.2 Microtubule-Organizing Centers and Associated Proteins	47
6.2.3 Motor Proteins	48
6.3 Intermediate Filaments	49
Chapter 7. Cell Lines	51
7.1 Basics of Cell Motility	51
7.2 Fibroblasts	54
7.2.1 Fibroblast Locomotion	55
7.2.2 Cell Culture	57
7.3 Keratocytes	58
7.3.1 Keratocyte Locomotion	59

Chapter 8. <i>In vivo</i> Experiment	61
8.1 Setup	61
8.2 Sample Preparation	64
8.3 Procedure and Results	65
Chapter 9. Conclusion and Outlook	73
Appendices	76
Appendix A. Actin Sample Preparation	77
Appendix B. List of Chemicals	78
Appendix C. Cell Medium	79
Appendix D. Fibroblast Culture	81
D.1 Thawing	81
D.2 Passaging and Plating	82
D.3 Freezing	83
Bibliography	85
Vita	90

List of Tables

2.1	Rate constants and critical concentration for plus and minus end	12
4.1	Numbers for polarizability of actin	30
4.2	Numbers for dipole force	31
B.1	Chemicals for cell culture	78

List of Figures

2.1	Model of atomic structure of monomeric actin	7
2.2	Structure of F-actin	8
2.3	Polarity of F-actin	9
2.4	Assembly of actin	9
2.5	Time course of polymerization	11
2.6	Time course of actin polymerization at different temperatures	15
2.7	Extent of actin polymerization versus temperature	15
3.1	TRITC-phalloidin labelled actin filaments visualized by fluorescence microscopy	21
3.2	Transmission spectra of various filters	22
3.3	Thermo-electric cooling	23
3.4	Setup of <i>in vitro</i> experiment	24
3.5	Transmission spectrum of dichroic mirror 560DCLP	25
3.6	x-y control by two rotation stages	26
4.1	Dipole force	32
4.2	Potential well depth	33
4.3	Concentration simulation	35
6.1	Actin stain of fibroblasts	41
6.2	Actin filament bundles and networks	41
6.3	Actin-myosin motility	45
6.4	Assembly of microtubules	47
7.1	Cell motility steps	52
7.2	Force for protrusion	53
7.3	Cultured SV-T2 cell	55
7.4	Fibroblast locomotion	56

7.5	Goldfish keratocyte	58
7.6	Dynamic network contraction	60
8.1	Laser system and pathway of laser beam	61
8.2	Setup for experiments on fibroblasts and keratocytes	62
8.3	Sample dish	64
8.4	Experiment with PDGF-BB treated SV-T2 cells	67
8.5	Another experiment with PDGF-BB treated SV-T2 cells	69
8.6	Experiment with a keratocyte of a dalmation molly	71
8.7	Experiment with PC-12 neurons	72

Chapter 1

Introduction

It is recently discovered that guiding of neuronal growth cones with laser light is possible [1]. This ability may play an important role in a variety of fields like neuroscience, cell biology, and biophysics. The guiding is done with a laser spot, placed in front of the nerve's leading edge to enhance growth into the beam focus. This results in controlling the growth direction of the growth cone. The optical tweezer, which uses the dipole-, or gradient-, force of a laser to trap and move particles, such as bacteria, is a useful tool in scientific fields, e.g., atom physics and biology. The guiding mechanism for the growth cones, however, is not based on this conventional tweezing effect as indicated by the fact that holding or moving of the cell was not possible. Two feasible explanations for the enhanced lamellipodia extension induced by weak optical forces are considered. One of them is enhanced actin polymerization in the leading edge. A laser produces a dipole force on a polarizable sample. The dipole force,

$$\vec{F}(\vec{x}, t) = \frac{1}{2}\alpha\nabla\vec{E}^2(\vec{x}, t), \quad (1.1)$$

is the force due to the interaction of the dipole induced by the electric field from the laser and the electric field itself. Here, the polarizability (α) of

actin determines the strength of this force. The result is an increase of actin monomers and oligomers in the beam spot. Although concentration enhancement and force are very small there will be a net flux of actin monomers and oligomers into the beam focus (see § 4.2). This might influence the lamellipodia to grow in the direction of the optically increased actin density. The calculated drift velocity for actin monomers in the cytoplasm is close to the observed growth rates of an active growth cone. Additionally, it is conceivable that the optical forces pull on the crosslinked filaments of the actin cortex and relieve pressure at the rearward cortex-microtubule junction, thus enhancing the pressure-dependent microtubule polymerization [1, 42]. Since lamellipodia extension, a process which underlies all motile cells, is influenced by the laser, the question arises if optical guidance may act as a general cell guidance method. We want to investigate this issue.

In performing an experiment on light-induced actin polymerization *in vitro* (Part I), we try to control and bias the polymerization process. Additionally, we hope to sustain the hypothesis that enhanced actin polymerization is the main reason for the success of the neuronal growth cone guiding experiment. Unfortunately, the *in vitro* experiment does not give more information about responsible mechanisms in growth cone guiding. Therefore another approach is taken, by doing “optical guiding” experiments with other cell types (Part II). Fibroblasts, which are also slow moving cells like neurons, and keratocytes, a fast crawling cell type, are used in these experiments. From knowledge of their motility behavior and response to the laser light, we hope

to gain a deeper insight into the underlying processes in cell motility.

Part I

Light-induced Actin Polymerization

Chapter 2

About Actin

2.1 General Information about Actin

The protein actin is expressed in nearly all types of eukaryotic cells. It is one of the most abundant proteins in human tissues and can be assembled into a variety of structures. In muscle cells, actin forms linear polymers which form the thin filaments of the sarcomere. In other cell types, actin also takes a variety of other forms. These forms include contractile filament bundles (stress fibres), highly organized parallel arrays of filaments in microvilli, isotropic networks of filaments within the cytoskeleton, as well as protein complexes (e.g. actomyosin) and monomers or small oligomers in the cytoplasm [36].

Actin is a ubiquitous protein which provides mechanical strength to the cell cortex. It acts as a transmitter of internal mechanical stresses and assists in the spatial organization of the cytoplasm. Actin also serves as a pathway for signal transduction and is responsible for the regulation of certain enzymatic activities within cells [25, 16].

Actin is a highly conserved protein in the sense that its sequence identity differs by less than 5 % between cytoplasmic actin, muscle actin and protozoan actin. Human actin is expressed by six proteins, distinct only by a

small residue. The human muscle form is identical to that in rabbits, mice, rats, chickens and cows.

2.2 Actin Monomers

Actin in monomeric form is called G-actin (globular actin). It is a single chain polypeptide with 375 amino acids and its molecular weight (MW) is 43000 u. The structure of free monomeric actin is not known yet. It has been difficult to obtain 3D crystals of pure actin appropriate for X-ray diffraction analysis because conditions favoring crystallization of G-actin also induce its polymerization into F-actin (filamentous actin) [32]. One can overcome this problem by complexing actin with proteins like DNase I, gelsolin S1, or profilin. These inhibit its polymerization and therefore form co-crystals. Fig. 2.1 shows a three-dimensional model of G-actin derived through X-ray diffraction. The crystallographic analysis shows that monomeric actin is separated into two lobes by a deep cleft. Each lobe consists of a five-stranded beta-sheet of identical topology. The lobes and the cleft comprise an adenine nucleotide, either ATP (adenine triphosphate) or ADP (adenine diphosphate), and a divalent cation, like Mg^{2+} or Ca^{2+} , bound by ionic and hydrogen bonds to amino acid side chains. Each of the two major domains is subdivided into two additional subdomains, numbered I-IV, where the C- and N-termini are located in subdomain I (see Fig. 2.1).

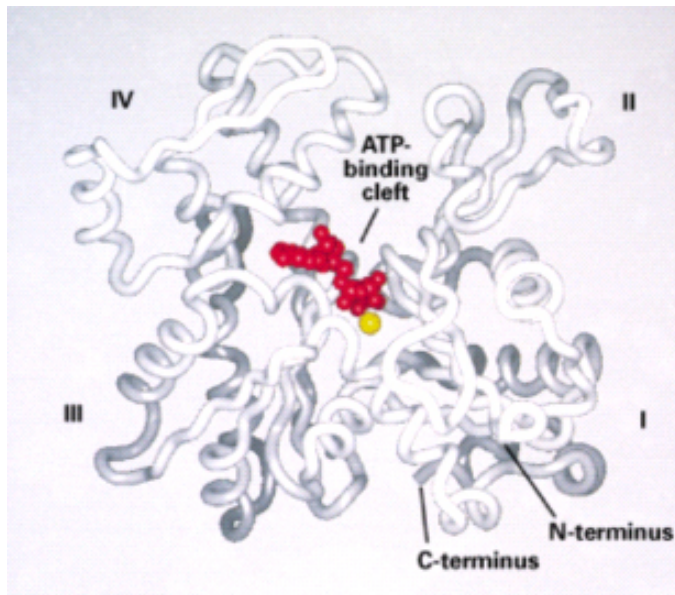


Figure 2.1: Atomic structure of a β -actin monomer from a nonmuscle cell (dimensions: $5.5 \text{ nm} \times 5.5 \text{ nm} \times 3.5 \text{ nm}$. ATP is shown in red, and Mg^{2+} is shown as a yellow ball. The subdomains are numbered from I-IV. From ref. [18].

2.3 Structure of F-Actin

Filamentous actin can be described by two models: as a single, tightly wound left-handed helix or as two right-handed helices of a long pitch. Only a short description of the latter model is given [32]. F-actin is formed by a tight helix of globular actin. This double right-handed helix consists of 13 subunits per turn. Assuming a subunit of 5.5 nm , the pitch is 71.5 nm . The two long-pitch helices are staggered by 2.75 nm and cross every 35.75 nm .

Actin filaments have a diameter of about 10 nm and they are typically several micrometers long. The structure of F-actin, as shown in Fig. 2.2, is

derived from X-ray diffraction and electron microscopy (EM) . The asymmetry

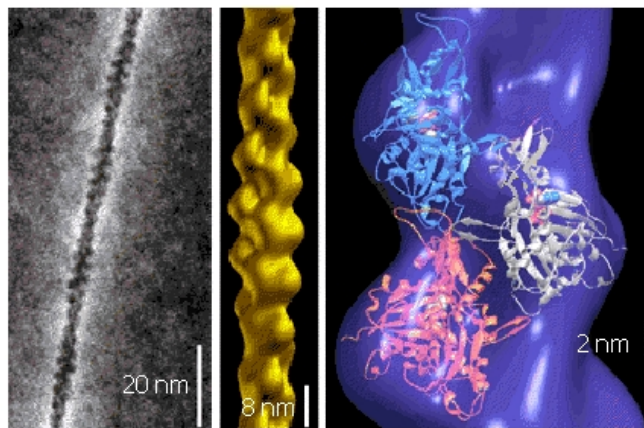


Figure 2.2: The structure of the actin monomer obtained from the actin-DNase I crystal is superimposed on the density map of the actin filament derived from X-ray diffraction and electron microscopy (EM). From ref. [41].

of the monomers and the polymerization process affect the structure of the filament, which is therefore, also asymmetric. The subunits assemble into F-actin by always attaching to the filament ends in the same orientation with respect to the filament axis. This results in a directional polarity of the filaments, which can be visualized by EM in negative stain preparations. There, the filaments have an arrowhead appearance, as can be seen in Fig. 2.3. From this arrowhead appearance, the filament ends were coined as barbed and pointed ends. In the literature, one also finds the terms (+)-end, or fast growing-end, and (-)-end, or slow growing-end, which represent barbed and pointed ends respectively.

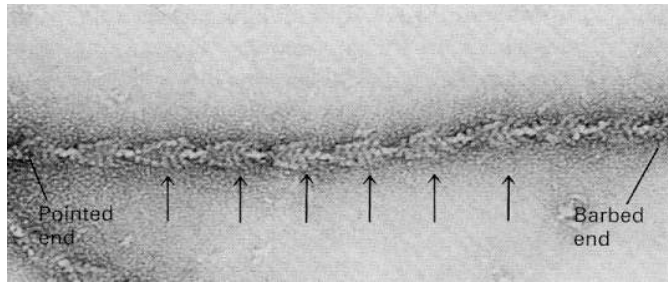


Figure 2.3: Polarity of F-actin: The filament polarity can be visualized by EM of F-actin bound to myosin S1 fragments. These S1 decorated actin filaments have an arrowhead appearance in negative stain preparations. \Rightarrow pointed and barbed end; from ref. [18].

2.4 Kinetics of Polymerization

2.4.1 Nucleation and Elongation

The assembly of G-actin into filamentous actin occurs in a two-step process, illustrated in Fig. 2.4. In the first step, actin monomers form into

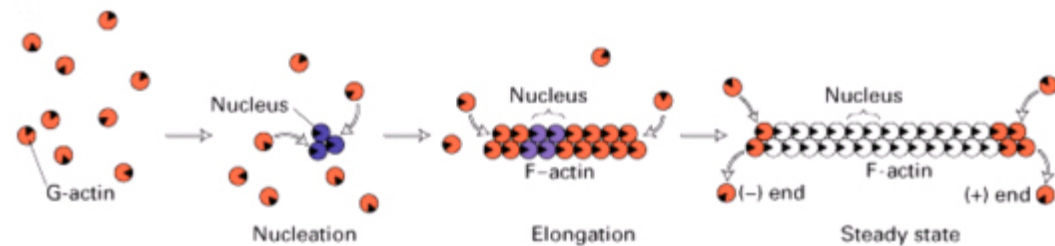


Figure 2.4: Assembly of actin; ATP-G-Actin is red, the actin complex is purple, and ADP-F-Actin is shown in white. From ref. [18].

stable oligomeric nuclei. This stability means that such a nucleus is more likely to grow into a filament than to dissociate into monomers. It can be expressed by a rate constant for nucleus formation k_N and one for dissociation

of the nucleus k'_N . Here, N represents the number of subunits in the nucleus. Kinetic analysis of polymerization curves indicate that the minimum size for a stable nucleus is a trimer [7, 44] but some evidence for a tetramer also exists [36]. In the second step, actin monomers bind to the nuclei to elongate the filament. This model of a nucleation-elongation mechanism was established by Engel and Wegner [3]. The assumption is that the rate constants k for addition of a monomer and k' for dissociation of a monomer are independent of oligomer size. A consequence of this nucleation-elongation model is that at steady state, there is a constant concentration of G-actin, called the critical concentration, c_{crit} . Below this, polymerization does not happen and above it, the polymer concentration equals the total initial actin concentration minus the critical concentration. Mathematically, c_{crit} is defined as k/k' . This critical actin monomer concentration depends on several factors (e.g., ionic strength) and ranges usually between $0.01 \mu\text{M}$ to $1 \mu\text{M}$.

2.4.2 Time Evolution of Actin Polymerization

The polymerization of G-actin into F-actin can be divided into three distinct time phases as shown in Fig. 2.5. The initial nucleation or lag phase involves fast monomer activation, where monomers bind to adenine nucleotides and divalent cations, and also the rate limiting step of nucleus formation. The much faster growth or elongation phase consists of rapid subunit addition to the nuclei. Here, the relationship between polymer elongation and time is approximately linear. When the system reaches steady state, the monomer

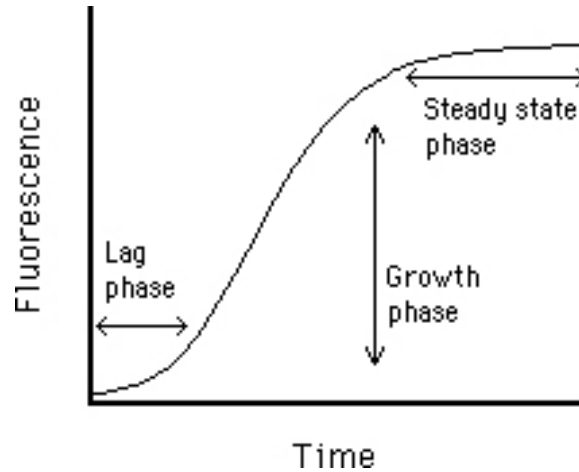


Figure 2.5: Fluorescence signal of labelled actin filaments versus time; from ref. [12].

and polymer concentrations stay invariant and the monomer concentration equals the critical concentration for polymerization. Subunit exchange between monomers and polymers continues, where subunits separate from the filament and other subunits attach to it. This subunit flux through the actin filament is called “treadmilling”. Thereby the average length of the filament remains unchanged (see also section 2.4.3).

As was mentioned above, the actin molecule is stabilized by a tightly bound adenine nucleotide (i.e., ATP or ADP) and its associated divalent cation (e.g., Mg^{2+} or Ca^{2+}). At first glance, treadmilling seems to violate the laws of thermodynamics, but the polymerization of actin with bound ATP dissipates chemical energy via ATP hydrolysis and is therefore not strictly reversible [7, 32]. Consistent with this result, it was first mentioned by Wegner [2] that,

under conditions where ATP-G-actin polymerizes, the net rates of addition and dissociation could be different at the two ends. Therefore at steady state, subunits would add up preferentially at one end and dissociate from the other end.

2.4.3 ATP- and ADP-Actin Assembly

In the assembly mechanism, G-actin containing ATP binds to the preferred filament end. ATP is hydrolyzed to ADP and phosphate, still bound to the actin, followed by the release of the phosphate to form a mixture of ADP-actin and ADP-P_i-actin subunits within the filament [36]. ADP-G-actin also polymerizes into filaments but at a much slower rate and higher critical concentration c_{crit} than ATP-G-actin. There are also differences in the affinity of ATP-G-actin and ADP-G-actin for the barbed and pointed ends. Table 2.1 shows typical rate constants and critical concentrations at the different filament ends. If the actual concentration is higher than the critical

Monomer in solution	barbed end		pointed end		c_{crit}^+	c_{crit}^-
	k_{on}^+	k_{off}^+	k_{on}^-	k_{off}^-		
ATP-G-actin	11.6±1.2	1.4±0.8	1.3±0.2	0.8±0.3	0.12±0.07	0.6±0.17
ADP-G-actin	3.8	7.2	0.16	0.27	1.9	1.7

Table 2.1: Rate constants and critical concentration for plus and minus end; units are $(\mu\text{M} \cdot \text{s})^{-1}$ for k_{on} , s^{-1} for k_{off} and μM for c_{crit} ; data is taken from ref.[47].

concentrations c_{crit}^\pm of the two ends, the filament will elongate on both sides,

whereas if it is lower than c_{crit}^{\pm} on both ends, the filament is likely to disassemble. Treadmilling occurs when the concentration is between c_{crit}^{+} and c_{crit}^{-} so that actin subunits dissociate from the pointed end and add up at the barbed end. Here, the length of the filament remains the same.

2.4.4 Influences on Actin Polymerization

In vitro, actin polymerization is strongly influenced by several environmental factors such as pH, ionic strength, and temperature. For instance, actin polymerization is more favored at lower pH due largely to induced preference of actin dimer formation and to salt-induced conformation by protons. The extent of actin dimer formation increases by two orders of magnitude, going from pH 8 to 6 at a temperature of 20 °C. The formation of a trimer is little affected. The lag phase (§ 2.4.2) becomes shorter and the rate of polymerization increases [11]. The critical concentration for filament formation is also decreased at lower pH.

The species and concentration of cation present also have an effect on the polymerization process. Mg^{2+} is preferred to Ca^{2+} and the higher the cation concentration, the lower the critical concentration for actin filament formation.

The largest effect on the mechanism of actin polymerization usually is its dependence on temperature, where dimer formation is the most sensitive step. The ratio of rate constants for assembly and disassembly changes four orders of magnitude between 10 to 35 °C. Above this temperature change,

the critical concentration remains almost the same. All ratios of forward and reverse rate constants change seven fold or less [10]. Fig. 2.6 shows the time course of actin polymerization by fluorescence increase at three different temperatures: 30 °C, 20 °C, and 10 °C from left to right. Fig. 2.7 shows the extent of polymerization versus temperature. Note the steep slope between 25 °C and 40 °C.

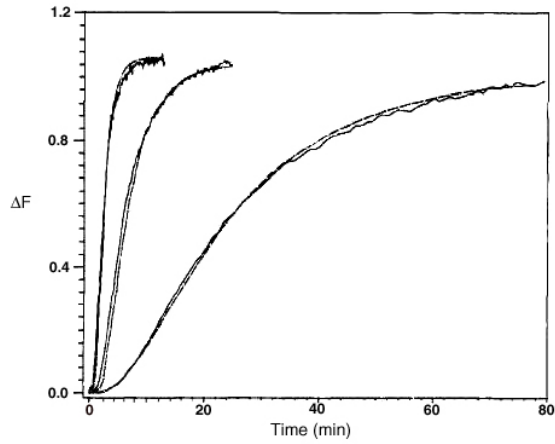


Figure 2.6: Time course of actin polymerization at 30 °C, 20 °C, and 10 °C from left to right. The solid lines show the fluorescence increase associated with the polymerization of 23.5 μM Ca-G-actin (pyrene labelled) in G-buffer initiated by the addition of 2 mM MgCl_2 . The dashed lines are computer simulated time courses. From ref. [10].

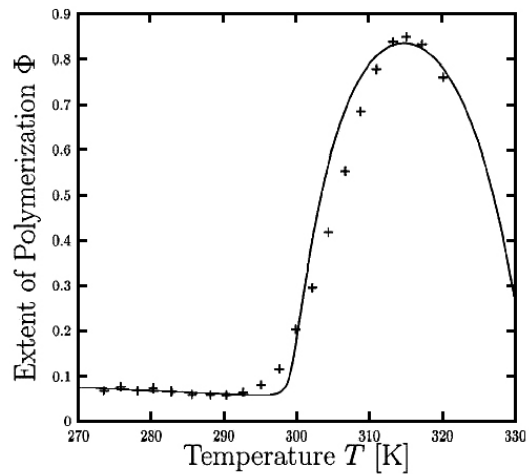


Figure 2.7: Extent of actin polymerization versus temperature. Plus symbols are experimental data (2 mg/ml of actin and 9 mM of KCl), and the solid line is a theoretical fit. From ref.[37].

Chapter 3

In vitro Experiment

3.1 Light-induced Actin Polymerization

In a homogenous G-ATP-actin solution with high enough salt concentration, actin starts to polymerize into filaments. In this case no region in the sample is more in favor of polymerization than another. After the system reaches steady state, one can ideally think of randomly distributed filaments.

The goal in this experiment was enhancement of actin polymerization in a certain region and, by that, control and “guidance” of polymerization. To achieve this, we tried to influence the polymerization process with the assistance of laser light. The basic principle is simple: the laser spot produces a dipole force on the sample. This is due to the fact that monomeric actin is polarizable, which determines, in part, the strength of the force. The result is an increase of the concentration of G-actin in the beam spot. More detailed explanations and calculations about the polarizability and the dipole force are given in § 4.1 and § 4.2. By scanning the beam over a certain width, we hoped to be able to visualize the concentration enhancement by fluorescence microscopy. Unfortunately, we could not observe such an effect in these experiments. The setup of the system and the preparation of the sample was

subsequently improved, without success. After these efforts, a theoretical approach was taken, which will be given in Chapter 4. It is apparent that the concentration enhancement in the region of the laser beam was too small to be seen clearly.

3.2 Experimental Procedure

3.2.1 Preparation of Sample

Monomeric actin was purified from rabbit skeletal muscle by the method of Spudich and Watt. It was rapidly frozen in liquid N₂ and then stored at -80 °C. On the day of use, aliquots of actin were thawed at room temperature. The actual sample preparation is done the following way:

- ***Antibleach***

Fluorescence microscopy is used to observe TRITC-phalloidin labelled actin filaments. In addition, we use “antibleach”. This binds to the dye and reduces bleaching, to obtain longer observation times. The antibleach procedure is given in Appendix A.

- ***Labelling of actin***

The high binding constant of rhodamine-phalloidin to actin filaments makes it easy to fluorescently label actin. However, one has to be aware of the fact that the bound phalloidin changes certain properties of F-actin. The binding of phalloidin prevents nucleotide hydrolysis from the high affinity binding site and drastically slows monomer exchange [22, 21].

Treadmilling is strongly inhibited in the presence of phalloidin and most actin is in a filamentous state. This, however, affects the purpose of this experiment by enhancing the formation of stable nuclei and small filaments. The polarizabilities of the actin subunits in oligomers add up, resulting in a stronger dipole force.

Using the recipe, given in Appendix A, one ends up with a 1 mg/ml actin solution. It is important to check that the TRITC-phalloidin aliquot is colorless. If it is exposed to long to air, it turns pink. This indicates that the dye will not fulfill its purpose any more. As soon as the dye is added, we protect the sample against light as well as possible, to prevent precocious bleaching. During the mixing steps, effort is made to keep the sample cooled in ice in order to slow the polymerization process.

- ***Dilution***

We mix the Antibleach with the labelled actin to reduce bleaching. As a supplementary possibility, a desired concentration of G-actin in the sample can be chosen. Usually we want to end up near the critical concentration of G-actin (0.01 to 0.1 mg/ml), which we try to achieve by mixing the labelled actin solution with antibleach in ratios between 1:10 and 1:100.

In order to initiate the polymerization process of actin as late as possible the sample is prepared a little differently. The label step is done similarly, except for exclusion of the actin. We continue with the dilution step and finally add

the missing fractional amount of G-actin.

For example to obtain a 0.02 mg/ml actin solution, the procedure is:

- * Put 196 μl of antibleach in 1.5 ml Eppendorf tube.
- * Add 3 μl of labelled actin solution (without actin).
- * Add 1 μl of G-actin and mix it well.

In the actual experiment, we did not begin with so many pre-polymerized filaments in comparison to the other preparation method.

- ***Sample on coverglass***

In the final step, the cold sample ($\approx 40 \mu\text{l}$) is placed between a cooled glass microscope slide and a cover slip. The cover slide is cooled by a TEC (Thermo-Electric-Cooler), see § 3.2.3. The slide is sealed with vacuum grease, which also provides a spacing of 20–80 μm between the slide and the cover glass [20]. To prevent adhesion of actin filaments at the glass surface, the surfaces are coated with albumin solution (incubation time ~ 20 min) to saturate it. On the other hand, we do also experiments without coating, so that the actin filaments are able to stick to the glass surfaces.

3.2.2 Fluorescence Microscopy

A general misunderstanding is that the smallest objects which can be seen in a light microscope are at least as large as half the wavelength of the used light source. The range of visible light is about 300–800 nm which means that

visible structures have to be of the order of several hundreds of nanometers [21]. However single fluorescently labelled actin filaments which have a diameter of ~ 10 nm can be seen in the fluorescence microscope (Fig.3.1). The optical law $0.61 \lambda/A$ (λ : wavelength, A : numerical aperture), derived by Helmholtz and Abbe, makes predictions about the resolution of two point sources as separate objects but does not say anything about the limits of visibility of single objects in the microscope. In fact, the visibility is limited by the signal to noise ratio. The maximum of the diffraction pattern of each object in the microscope has to be distinctively above the background noise level [21]. Even tagged particles of the size of a few nanometers can be seen in the microscope, if they provide an optical signal, which is strong enough, to overcome the background, subject to the condition that these particles are separated enough from each other.

For visualization of actin filaments by fluorescence microscopy, see Fig. 3.1, phalloidin labelled with a fluorescent chromophore, in our case TRITC, is used. The dye absorbs a certain wavelength and emits light at another, longer wavelength. This sort of rhodamine has excitation spectra with peak wavelength around 550 nm and maximum emission wavelength around 570 nm. A good signal to noise ratio is achieved by using an appropriate fluorescence filter set which guarantees a low background light level. The Zeiss HBO100W/2, a high pressure mercury arc lamp is used as light source. A narrow excitation filter (D540/25x from Chroma Technology Corp.) with a center wavelength of 540 nm and a bandwidth of 25 nm was placed in front of it (see blue curve in Fig. 3.2). The transmission efficiency of this filter is around 80 %. Underneath

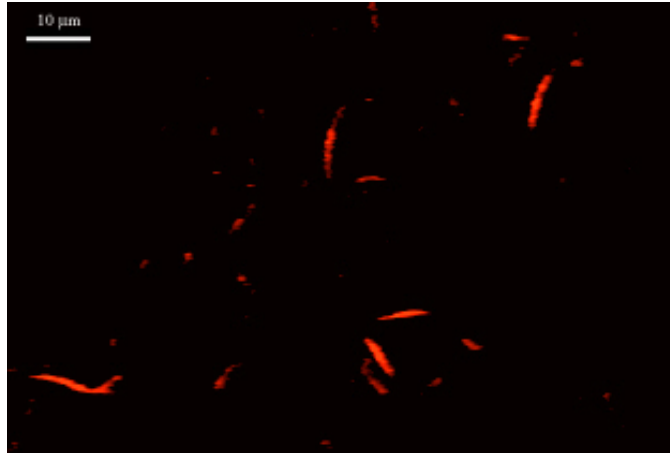


Figure 3.1: TRITC-phalloidin labelled actin filaments visualized by fluorescence microscopy. Labelled actin was polymerized for 30 min at a concentration of 1 mg/ml, followed by a 1 : 1500 dilution with antibleach. Actin filaments of different sizes and shapes can be seen.

the objective-revolver, a filter cube equipped with a beam splitter (51011bs from Chroma Technology Corp.) and an emission filter (HQ 585/40m from Chroma Technology Corp.) is used. The beam splitter reflects the excitation light (540 nm) to $\sim 85\%$ and transmits the emitted light (570 nm) from the fluorescently labelled F-actin to $\sim 75\%$ (see green curve in Fig. 3.2). The emitted light passes then an emission filter with a center wavelength of 585 nm and a bandwidth of 40 nm with an efficiency of $\sim 85\%$ (see red curve in Fig. 3.2).

3.2.3 Cooling of Sample

Thermo-electric effects in semiconductors cause currents to flow due to temperature gradients but also cause temperature gradients when an electrical

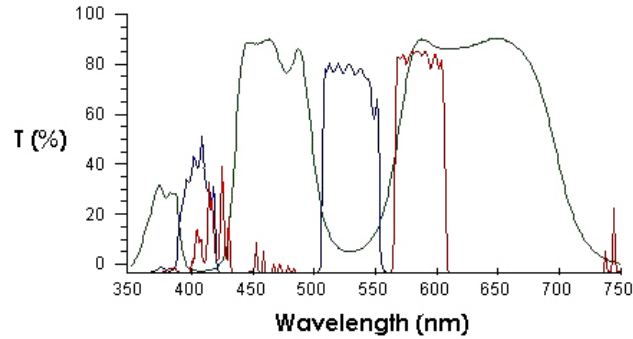


Figure 3.2: Transmission spectrum of excitation filter (blue curve), beam splitter (green curve) and emission filter (red curve); from ref. [8].

current is applied [5]. The thermo-electric cooler (TEC) is a device in which a current is applied to a semiconductor causing a temperature reduction and cooling. Such thermo-electric cooler consist of multiple semiconductor elements, which are connected in series as shown in Fig. 3.3.

The TEC (CP 0.8-63-06L from Melcor), is glued with thermal epoxy to a piece of aluminum, which can be mounted on a cover slide. A cut in the aluminum clears a space for a glass probe thermistor (121-502EAJ-Q01 from Fenwal Electronics), which is fixed there with thermal epoxy. On top of the TEC a heat sink with additional fan is attached. The sample is cooled to temperatures between 4 – 20 °C, which is easily achieved by this setup. The thermistor is connected to a conventional multimeter, where the resistance is read out. Such a thermistor has a characteristic R-T curve, which allows identification of the actual temperature.

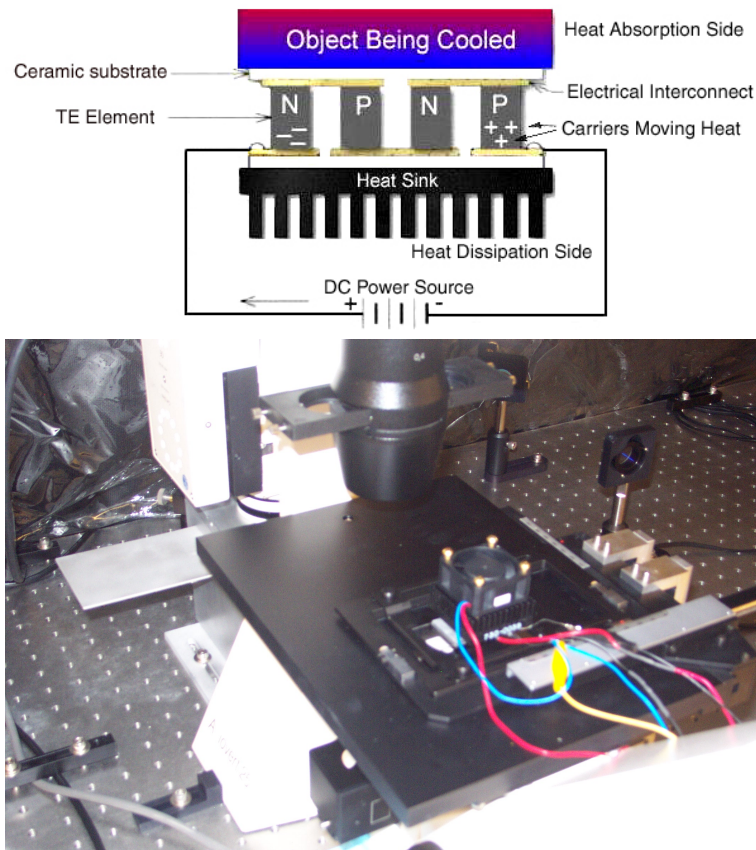


Figure 3.3: Thermo-electric cooling: upper picture shows basic setup of a TEC. The TE element with ceramic surfaces is connected on one side to the object being cooled and on the other side to a heatsink. From ref. [6]. The lower picture shows the experimental realization with additional fan on top of a heatsink.

3.3 Experimental Setup

Fig. 3.4 shows the actual experimental setup including the laser system. Fluorescence microscopy is performed with an inverted Zeiss microscope (Axiovert 25) equipped with a 63x objective (Zeiss Plan Neofluor, Ph3, NA=1.25),

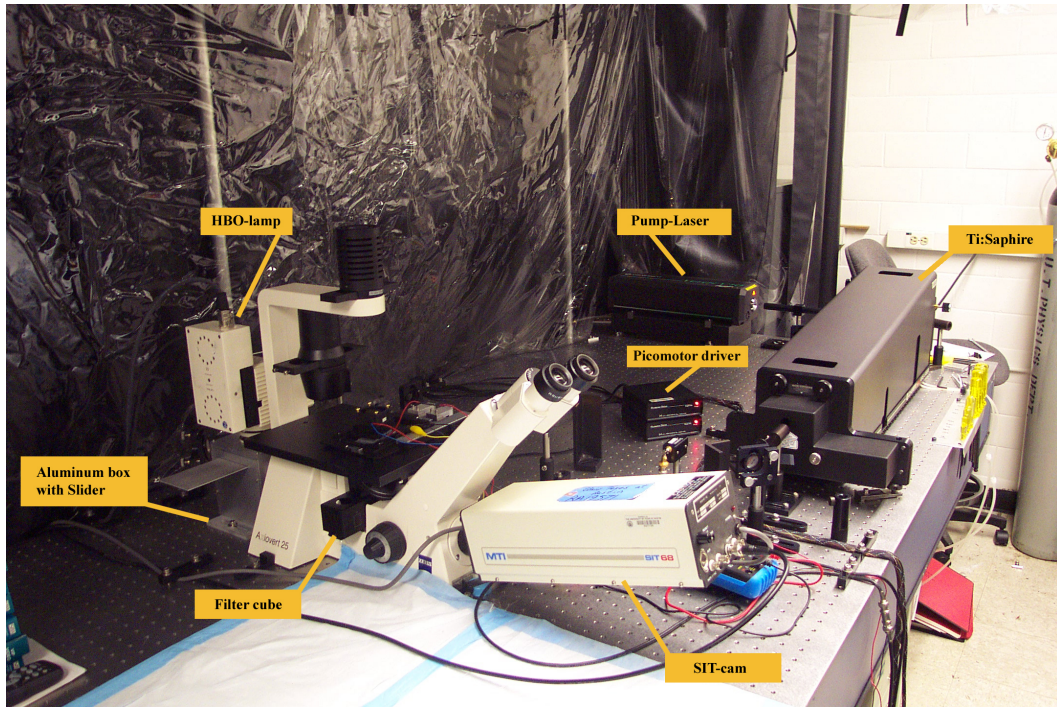


Figure 3.4: Setup of *in vitro* experiment with laser system, consisting of a Verdi (pump laser) and a Ti:Sapphire. HBO lamp provides the excitation light for fluorescence microscopy. Imaging is done with the SIT-camera.

a Zeiss HBO100W/2 light source and a special filter set for simultaneous rhodamine fluorescence and laser observation. Typical wavelengths used in laser applications with biological materials are in the region of the near infrared because biological materials have low absorption rates in this spectrum. The laser system we use is a Ti:Sapphire, pumped by a Verdi (both from Coherent), with an output wavelength of 800 nm. Maximum power output of the Ti:Sapphire is 1.86 W when pumping it with 10 W of the Verdi, which is the usual pump power. The actual laser power is controlled by an AOM

(acousto-optic modulator from Intra-action Corp.) with a maximum efficiency of $\sim 75\%$ which means in terms of power $\approx 1.4\text{ W}$. After the AOM, the laser beam combines with the green filtered HBO light (see § 3.2.2) by a dichroic mirror (560DCLP or XF2016 from Omega Optical incorporated) and enters the microscope through the back port of the microscope (usually used for HBO lamp). Fig. 3.5 shows the transmission spectrum of this dichroic mirror. The

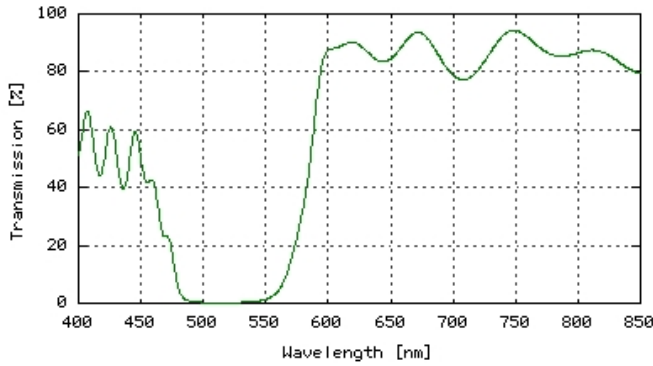


Figure 3.5: Transmission spectrum of dichroic mirror 560DCLP. From ref. [34].

mirror is placed inside a home-built box. This aluminum box connects HBO-lamp and microscope. It has a hole in the back to let the laser beam pass through. A green filter (D540/25x) is inserted in the top of the box to achieve the appropriate excitation wavelength for the rhodamine. At each case a slot is cut in the two sides to insert a slider. With this structure, one can block or pass the green light very quickly and efficiently. Another dichroic mirror inside the filter cube, mentioned in § 3.2.2 reflects then the green and near infrared light for the most part and transmits red light to about 75 % (see green curve in Fig. 3.2). In addition to that an emission filter is used to get a cleaner signal. For imaging, the microscope is connected to a SIT-camera (SIT68 from MTI)

by a 0.5x c-mount (from Zeiss), whereby the signal is recorded on videotape by a VCR.

The microscope stage is controlled by two rotation stages, which are attached to the two stage knobs as shown in Fig. 3.6. The whole structure is

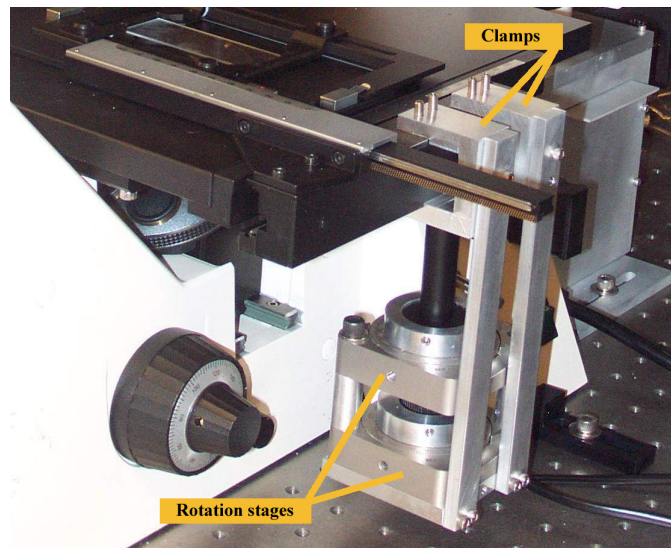


Figure 3.6: x-y control by two rotation stages, mounted on the microscope stage and held by clamps; parts to rotation stage were built by Dr. Valery Milner.

held by two clamps, which are connected to the microscope stage. This structure allows me to control x- and y-direction by steering the rotation stages with two independent function generators. These function generators are connected to picomotor drivers (from New focus), which are connected to the rotation stages. The outgoing signal of the function generators are translated by the picomotor drivers, whereby the amplitude determines the increment

and the frequency determines the duration of the steps. We can therefore “draw” simple shapes like lines, ellipses and circles.

The actual sample is placed on the microscope stage. A TEC can be mounted on top of the cover slide to keep the sample cold for a desired amount of time. We start the experiment with fluorescence microscopy only, where very few and short actin filaments can be seen. Then the excitation light is blocked by the slider (aluminum box) and the laser beam, controlled by a AOM, is allowed to make its way to the sample. Low laser power, such as ≈ 30 mW, is used in order to not damage the SIT-camera. The next step is to scan the sample in the desired path by running the function generators in a proper way. The light path to the SIT-cam is blocked before the laser power is increased to ≈ 400 mW. The actual “concentration” experiment is done for about 20 to 50 min before the laser power is lowered again and the beam path for the excitation light is reopened. Then the laser beam and the fluorescence signal is observed simultaneously, unfortunately as already mentioned without any conclusive results.

Chapter 4

Theoretical Approach to Actin Polymerization

4.1 Polarizability of Actin

In order to calculate the dipole force or the concentration variation induced by the laser beam one needs to know the polarizability of monomeric actin. We begin with an estimation of the refractive index of pure G-actin. By applying the appropriate Clausius-Mosotti equation, the polarizability is thereby obtained.

4.1.1 Refractive Index of G-actin

The key to estimating the refractive index of pure G-actin, n_{actin} , is the Gladstone-Dale rule [35]:

$$\frac{\partial n}{\partial c} = \bar{v}_{\text{P}}(n_{\text{P}} - n_0). \quad (4.1)$$

This equation relates the refractive index increment, $\partial n/\partial c$, of a polymer solution, the partial specific volume, \bar{v}_{P} , of a polymer and the refractive indices of the pure solvent and the pure protein. The partial specific volume of G-actin is $\bar{v}_{\text{actin}} = 0.75$ ml/g and was taken from ref. [33]. In order to obtain n_{actin} , the refractive index increment is needed.

In most cases, the alteration of the refractive index increment, $\partial n/\partial c$, of proteins is linear with λ^{-2} , where λ is the wavelength of the scattering light [30]:

$$\frac{\partial n}{\partial c}(\lambda) = A\lambda^{-2} + B. \quad (4.2)$$

In ref. [30], the increment for actomyosin in water is given at three different wavelengths. Assuming that this protein's conformation is close to that of G-actin, the refractive index increment for G-actin at $\lambda = 800$ nm is calculated by linear regression. The result is

$$\frac{\partial n}{\partial c}(800 \text{ nm}) = 0.19 \frac{\text{ml}}{\text{g}}. \quad (4.3)$$

Applying the Gladstone-Dale rule (Equation 4.1) with water as solvent ($n_w = 1.33$), results in the refractive index of pure G-actin:

$$n_{\text{actin}} = 1.59. \quad (4.4)$$

4.1.2 Polarizability

With the refractive index of G-actin, and therefore the dielectric number, $\epsilon_{\text{actin}} = n_{\text{actin}}^2$, we can calculate the polarizability by applying the Clausius-Mosotti equation [38] given by

$$\alpha = 4\pi\epsilon_0 a^3 \epsilon_w \frac{\epsilon_{\text{actin}} - \epsilon_w}{\epsilon_{\text{actin}} + 2\epsilon_w}. \quad (4.5)$$

This equation expresses the relation between the polarizability α of a single homogenous dielectric sphere (assumption), its dielectric number ϵ_{actin} , the

dielectric number of the surrounding medium ϵ_w , and the sphere's volume $V = \frac{4}{3}\pi a^3$. Table 4.1 shows the numbers which are used. As a result for the

Parameter	Value	Notation
ϵ_w	1.77	Dielectric number of water
ϵ_{actin}	2.51	Dielectric number of actin
a	$3.0 \cdot 10^{-9}$ m	Radius of gyration for monomeric actin
ϵ_0	$8.85 \cdot 10^{-12}$ F/m	Dielectric constant

Table 4.1: Numbers for polarizability of actin

polarizability for pure G-actin one gets:

$$\alpha = 6.5 \cdot 10^{-37} \frac{\text{Cm}^2}{\text{V}}. \quad (4.6)$$

4.2 Dipole Force

Starting with a homogenous distribution of actin monomers in a sample, the laser beam will induce a local concentration variation due to the dipole force. The dipole force, in a time averaged version [50], is given by

$$\vec{F}(r) = \frac{1}{2n} Z_0 \alpha \nabla I(r). \quad (4.7)$$

n is the refractive index of the medium (water), Z_0 , the impedance of free space, α , the polarizability of actin, and I , the intensity of the laser beam.

Assuming a Gaussian beam profile the intensity is given by:

$$I(r) = I_0 \exp\left[\frac{-2r^2}{\omega_0^2}\right]. \quad (4.8)$$

r is the radial distance from the center of the laser beam and ω_0 the spot size, which corresponds to the radial distance, where the intensity falls to e^{-2} . I_0 represents the maximum intensity and can be calculated by applying Equation 4.9,

$$I_0 = \frac{2P}{\pi\omega_0^2}, \quad (4.9)$$

where P is the power of the laser beam, which can easily be measured. Table 4.2 shows the parameters and values used in these calculations. Building

Parameter	Value	Notation
α	$6.5 \cdot 10^{-37} \text{ Cm}^2/\text{V}$	Polarizability
n_w	1.33	Refractive index of water
a	$3.0 \cdot 10^{-9} \text{ m}$	Radius of gyration for monomeric actin
Z_0	377Ω	Impedance of free space
P	0.45 W	Laser power
ω_0	$1.5 \cdot 10^{-6} \text{ m}$	Spot size
k_B	$1.38 \cdot 10^{-23} \text{ J/K}$	Boltzmann constant
T	300 K	Temperature
η	0.01 Pas	Viscosity

Table 4.2: Numbers for dipole force

the first derivative of the intensity (Equation 4.8) and plugging that, in addition to the numbers given in Table 4.2 into Equation 4.7, results in a dipole force profile, shown in Fig. 4.1. In order to get a better feeling for the strength of this force, the potential energy is shown in Fig. 4.2. The well depth in terms of energy divided by k_B is only ≈ 0.85 Kelvin. Thus the force is very small, but this situation can be compared with the flux of a current in a conductor. Actin monomers in a sample do their random walk due to thermal fluctuations

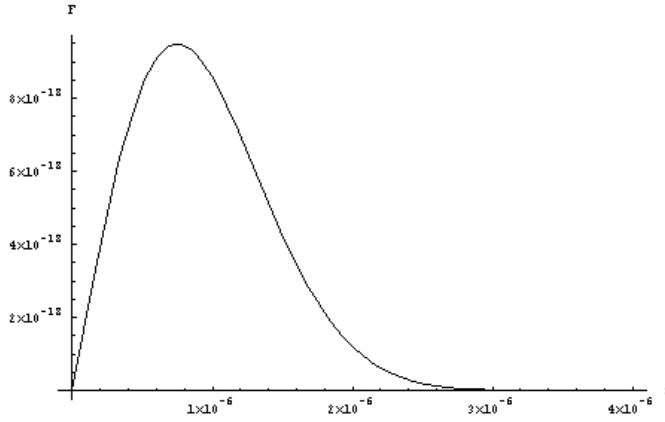


Figure 4.1: Dipole force F in units of N in dependence of radial distance r ranging from the center of the laser beam to $3 \cdot 10^{-6}$ m. The maximum is located at $\omega_0/2$.

like electrons do in a conducting wire. No matter what tiny amount of voltage one applies to a conducting wire, it always results in a net current flux. The actin monomers will therefore also drift with a certain velocity, v_{drift} , into the center of the laser beam.

In an aqueous actin sample the viscosity of the solution can vary to a large extent. We use in our calculations 0.01 Pas, which is in between the numbers given by ref. [17, 9]. The force due to Stokes friction is

$$\vec{F}(r) = \xi \vec{v}_{\text{drift}}(r) = 6\pi a \eta \vec{v}_{\text{drift}}(r), \quad (4.10)$$

where ξ is called the friction coefficient and a the radius of gyration. Hence one gets a maximal drift velocity for actin monomers of about 15 nm/s or 54 $\mu\text{m/hr}$.

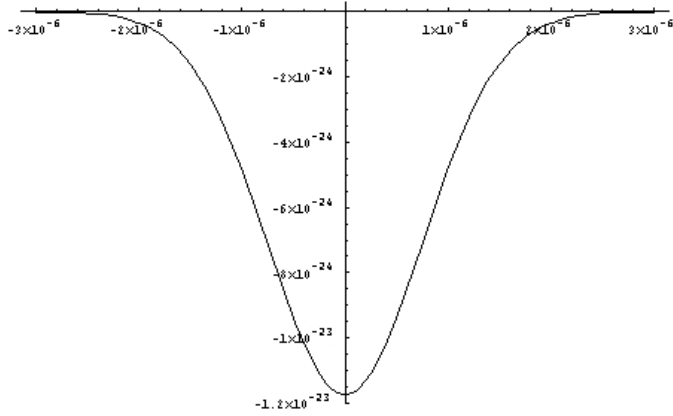


Figure 4.2: Potential energy U in Joule in dependence of the radial distance r in meters.

4.3 Concentration Enhancement

In § 4.2, I described the dipole force and calculated its actual profile. Here, I will discuss the effect on the concentration alteration in equilibrium state under influence of the laser. This will give information about the extent of the effect and its visibility by fluorescence microscopy.

The key to the following two-dimensional analysis is the diffusion equation [29], given by

$$\frac{\partial c(\vec{x}, t)}{\partial t} = \frac{\partial}{\partial x} \frac{1}{\xi} \left(k_B T \frac{\partial c(\vec{x}, t)}{\partial x} + c \frac{\partial U(\vec{x}, t)}{\partial x} \right), \quad (4.11)$$

which is called the Smoluchowski equation. Here, the time dependence does not play an important role and is estimated by the drift velocity, v_{drift} (see § 4.2). Therefore a reflection on the total flux, $j(\vec{x})$, of the system (see

Equation 4.12) is sufficient:

$$j(\vec{x}) = -D \frac{\partial c(\vec{x})}{\partial x} - \frac{c(\vec{x})}{\xi} \frac{\partial U(\vec{x})}{\partial x}. \quad (4.12)$$

$-D \frac{\partial c}{\partial x}$ describes the process of diffusion due to Fick's law, which says that if the concentration is not uniform, there is a flux which is proportional to the spatial gradient of the concentration. Note that the average velocity of the individual particles due to Brownian motion is zero [29]. The diffusion constant, D , which characterizes thermal motion, is related to the friction coefficient ξ , which specifies the response to the external force by the Einstein relation

$$D = \frac{k_B T}{\xi}. \quad (4.13)$$

The second factor in Equation 4.12 describes the additional flux due to the external force, which, in this case, is created by the laser.

In equilibrium state the total flux, j , must vanish:

$$-D \frac{\partial}{\partial x} c_{\text{eq}}(\vec{x}) - \frac{1}{\xi} c_{\text{eq}}(\vec{x}) \frac{\partial U(\vec{x})}{\partial x} = 0. \quad (4.14)$$

Solving this equation for $c_{\text{eq}}(\vec{x})$ with assistance of Equation 4.13 leads to

$$c_{\text{eq}}(\vec{x}) = c_0 \exp\left[-\frac{U(\vec{x})}{k_B T}\right], \quad (4.15)$$

where c_0 represents the initial concentration.

Using the potential, $U(\vec{x})$, of the laser with its Gaussian profile,

$$U(\vec{x}) = -\frac{\alpha Z_0 P}{\pi n_w \omega_0^2} \exp\left[-\frac{2\vec{x}^2}{\omega_0^2}\right], \quad (4.16)$$

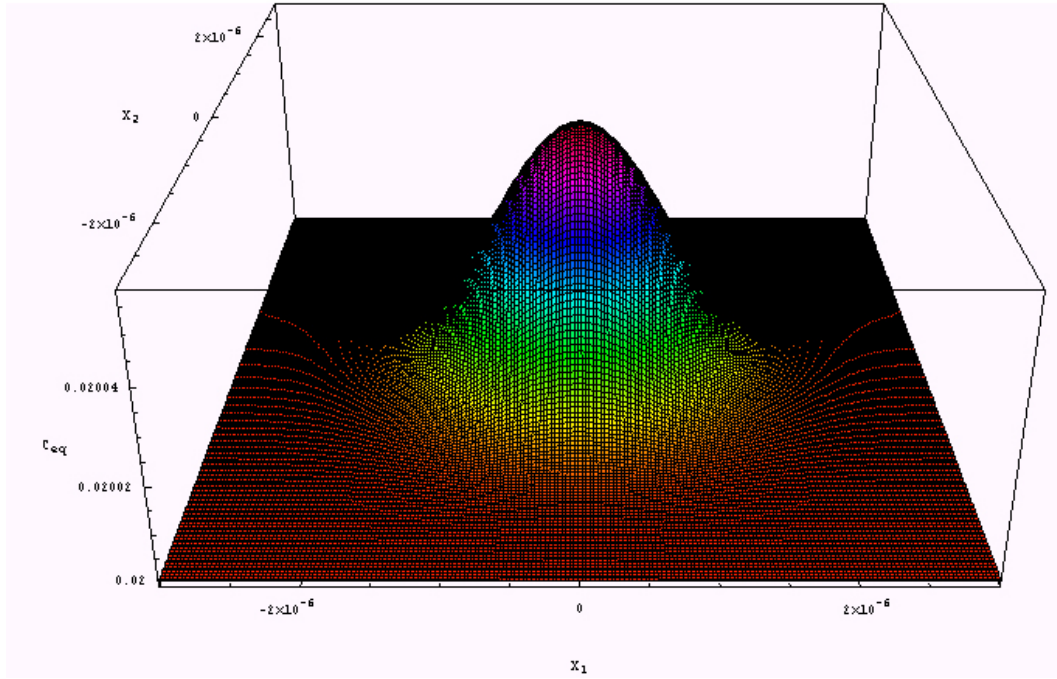


Figure 4.3: Simulation of concentration at equilibrium state with initial concentration of $c_0 = 0.2$ mg/ml.

and plugging in the corresponding values given in Table 4.2 has the following outcome for $c_{\text{eq}}(\vec{x})$, shown in Fig. 4.3. The concentration enhancement in the center of the laser beam is only ≈ 0.28 % which is almost negligible. Considering the fact that the effective intensity is even lower by scanning a line with the beam, one does not expect to observe a visible effect.

Chapter 5

Conclusion and Outlook

Due to the fact that the concentration enhancement in the beam spot is so small, it is not surprising that no clearly visible effect is observed. The effect of the concentration enhancement might be significant if the sample is prepared in a way that one is exactly at the critical concentration. Thus a little local increment of G-actin would be enough to introduce the polymerization process. This region may stand out from the background and can possibly be visualized by fluorescence microscopy. Unluckily it is very tough to achieve the critical concentration exactly. It would have been a very time consuming procedure (viscosimetry) for us, which we did not want to try. However, using synthetic actin from *Escherichia coli*, which is highly pure, maybe a possibility to overcome this problem. Once the critical concentration is determined, the purity of the actin ensures that this c_{crit} is valid every day for every experiment. By using synthetic actin and probably a more powerful laser, control of actin polymerization in vitro may be possible.

Actin polymerization may also be enhanced locally by a temperature effect. One can imagine to cool the sample, e.g., with a TEC, so that the extent of polymerization is in a highly sensitive region (Fig.2.7), where a few

degrees cause a large increase of polymerization. Using a visible laser, where the light is more absorbed than in the near infrared, with enough power heats the sample locally and causes an increase of polymerization in the beam spot. This might be a reasonable possibility to bias actin polymerization *in vitro*.

Although the actual experiment failed, it still seems reasonable that even a less powerful laser beam has enough influence to cause a local actin density increment in a cell, which may be enough to induce an enhanced growth of lamellipodia into the beam spot.

Part II

Optical Cell Guiding

Chapter 6

The Cytoskeleton of a Cell

The internal movements of a cell, such as the transport of membrane vesicles, are essential for growth and differentiation of a cell. Actual cell movements require fuel (ATP) and proteins that convert the energy stored in ATP into motion. The cytoskeleton, a cytoplasmic system of fibers, is involved in all movements of a cell. The cytoskeleton serves the cell as a stabilizing and structural element by supporting the cell membrane and by providing a framework to which organelles are attached. In addition, it is dynamic and generates movements by constantly rearranging its structure. The cytoskeleton is an internal network of three types of cytosol fibers: microfilaments, intermediate filaments, and microtubules. The intermediate filaments are the main structural determinants inside a cell but they are not known to produce any cell movements. Only microfilaments and microtubules are involved in cell motility. The following three Sections represent an overview about the cell's cytoskeleton. This summary is mainly composed of the subject matter of chapters 22 and 23 of ref. [18].

6.1 Microfilaments

6.1.1 The Actin Cytoskeleton

As mentioned in § 2.1 actin is found in nearly all eukaryotic cells and it is better known than any other protein in the cytoskeleton. Actin plays an important role in every type of motility [18]. The richest area of actin in a cell is the cortex, a narrow zone just beneath the plasma membrane. When looking at an electron micrograph or an actin stain of a cell, one can see that the actin cytoskeleton is organized in bundles and networks of filaments (Fig. 6.1), which build the framework that supports the plasma membrane and determines the cell shape.

The assembly of actin filaments starts with the formation of short and stable actin oligomers (nuclei), which rapidly elongate into filaments. The filaments form a steady-state equilibrium with the actin monomers and start treadmilling (see § 2.4). The actin filaments in networks and bundles are held together by actin-cross-linking proteins, whereby these proteins must have two actin-binding sites, one for each filament. The length and flexibility of a cross-linking protein critically determine whether networks or bundles are formed (Fig. 6.2). Short cross-linking proteins, such as fimbrin or α -actinin, pack actin filaments closely and force them to align in parallel arrays to form so-called bundles. Long and flexible cross-linking proteins, such as filamin, spectrin, and dystrophin are responsible for the formation of networks, where actin filaments crisscross and may take any configuration. Many crosslinking proteins contain a camodulin-like calcium binding domain. Calcium plays an

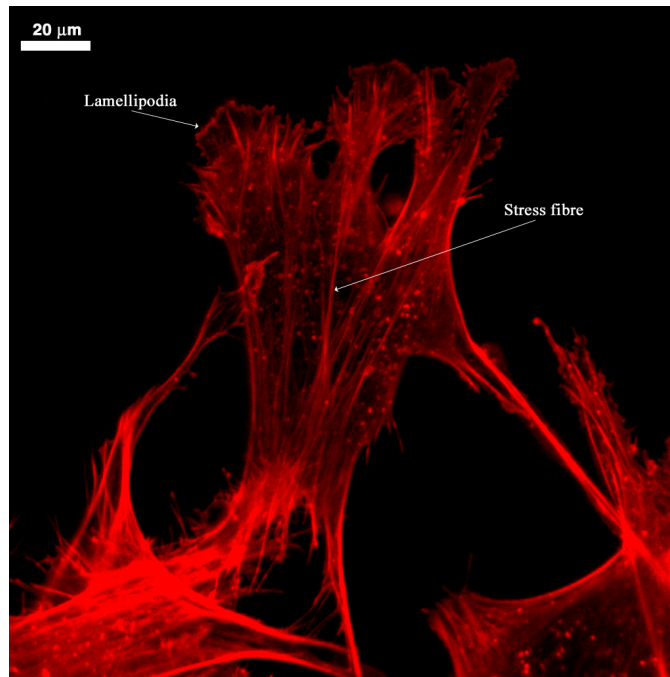


Figure 6.1: TRITC-phalloidin actin stain of fibroblasts, observed with LSM. One can see the actin enriched area near the leading edge. Also single stress fibres are visible.

important regulatory role by preventing these proteins from binding to actin filaments.

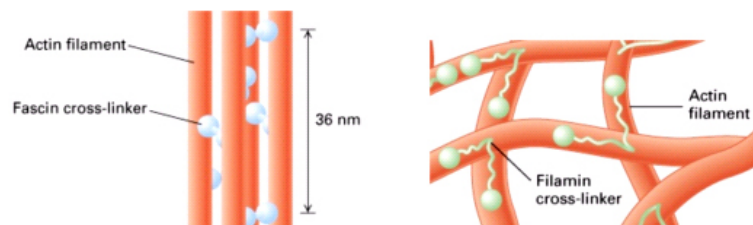


Figure 6.2: Actin filament bundles and networks, formed by different actin-cross-linking proteins. From ref. [18].

The shape of a cell is also determined by the proteins that connect the filaments to the membrane. These membrane-microfilament binding proteins can connect either directly to an actin filament or through more complex linkages. The membrane is held flat when it attaches to the filament network and it shows up in a fingerlike shape when it connects to the stiff filament bundles. Supported by the cytoskeleton, these cell-surface projections build a rigid structure.

There are two types of fingerlike membrane extensions, microvilli and filopodia, which are supported by an internal actin bundle. Microvilli are $0.5 - 10 \mu\text{m}$ long and are fairly stable in their size. In most microvilli the crosslinking protein fascin organizes actin filaments. In suspension (medium), microvilli increase the surface area available for absorption of molecules into a cell, since their primary function is the transportation of nutrients. Filopodia are responsible for the attachment of a cell to a solid surface. They are found at the leading edge of moving or spreading cells. Filopodia are transient structures. They are only present during the time required to establish a stable adhesion with the underlying substrate [18]. The crosslinking proteins are also fascin or filamin.

6.1.2 Actin Sequestering Proteins

In § 2.4 the dynamics of actin assembly *in vitro* and the factors that influence it have been discussed. *In vivo*, mechanisms other than variation of salt concentration or dilution play a part in promoting or inhibiting actin

polymerization. The cellular actin concentration is ~ 0.5 mM which is about 5000 times higher than the critical concentration *in vitro*. Therefore one would expect most of the actin in a filamentous state. Measurements however, show that about 40 % of the actin is unpolymerized [18]. A likely explanation is that small actin binding proteins in the cytosol sequester actin and hold it in a form that is unable to polymerize. Two proteins, thymosin β_4 and profilin, have emerged to control the assembly of actin [45]. Both of them build a 1:1 complex with an actin monomer. Thymosin β_4 (MW 5000 u) is unable to bind to F-actin and functions therefore as a buffer for monomeric actin. The 1:1 complex is in equilibrium with unbound thymosin β_4 , G-actin, and F-actin. For example, an increase of the concentration of the actin-sequestering protein would result in disassembly of actin filaments because the ratio between F-actin and G-actin will go back into its equilibrium state.

Profilin (MW 15000 u) binds an ATP-actin monomer to a stable 1:1 complex. It is the only actin binding protein that allows exchange of ATP for ADP. By binding to PIP₂, a membrane lipid, its activity to bind actin is inhibited. A current model signifies that profilin functions as a shuttle between G-actin and F-actin pools. It may regulate the store of unpolymerized actin by drawing actin from thymosin β_4 and releasing it to actin filaments [18].

6.1.3 Capping and Severing Proteins

Control over length of actin filaments is achieved by capping or severing proteins. These proteins are usually regulated by two signaling pathways, one

mediated by calcium and one by PIP_2 . Higher presence of calcium enhances the activity of capping and severing processes whereas higher presence of PIP_2 inhibits these activities.

Gelsolin, an actin severing protein, breaks all of the filaments in a network into short filaments by binding to the filaments, where it disrupts the bond between two subunits. It remains bound to the plus-end of one piece where it prevents actin subunit exchange.

Cap Z and tropomodulin are capping proteins whereby Cap Z covers the plus-end and tropomodulin the minus-end. The capability to cover plus- and minus-end of the same filament prevents an actin filament from depolymerizing.

6.1.4 Myosin

As mentioned in the beginning of this section the assembly of actin filaments is not the only process to bring about cell movements. Another mechanism for generating movements relies on an interaction between actin filaments and the motor protein myosin. Myosin is a family of mechanochemical enzymes, which convert energy derived from ATP hydrolysis into conformational changes. These allow myosin to walk along an actin filament [18], as illustrated in Fig. 6.3.

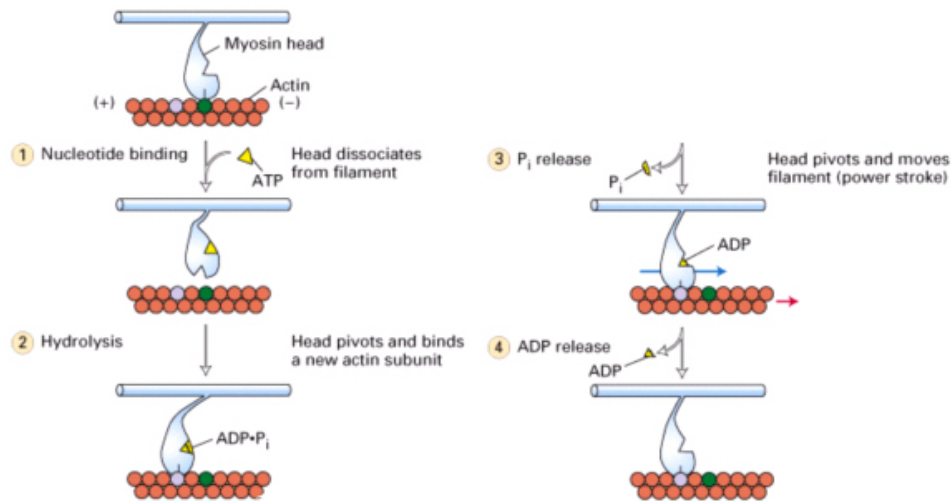


Figure 6.3: Actin-Myosin motility: Without any bound nucleotide myosin binds tightly to actin. As soon as myosin binds ATP the actin binding cleft is opened. Hydrolysis of ATP occurs and causes a movement of the myosin head to a new position before it rebinds to the filament. Myosin releases phosphate whereby the actual power stroke (force generation) happens. After that, ADP is released and the myosin returns to its rigid conformation. From ref. [18].

Myosin I (a monomer) and myosin V (a dimer) are involved in cytoskeleton-membrane interactions such as transport of membrane vesicles and movements of the plasma membrane. Myosin II (a dimer) powers muscle contraction and cytokinesis. All myosin are structured in head, neck, and tail domains. The head domain is responsible for actin- and ATP-binding activities, which are controlled by calmodulin-like subunits bound to the neck domain. The tail domain organizes myosin into a monomer or a dimer and it is also a critical determinant of the type of function of a myosin.

6.2 Microtubules

Microtubules are responsible for many cell movements, such as beating of flagella or transport of membrane vesicles in the cytoplasm. The movements can either be generated by polymerization or depolymerization of microtubules and by assistance of motor proteins. Additionally, microtubules also serve structural functions.

6.2.1 Composition and Assembly

A microtubule is a polymer composed of globular tubulin subunits which are arranged in a cylindrical tube measuring 24 nm in diameter. The subunit is a heterodimer consisting of one α - and one β -tubulin monomer, each measuring 4 nm in diameter. Each heterodimer binds two molecules of GTP (guanine triphosphate) nucleotide. α -tubulin binds GTP irreversibly whereby no hydrolysis occurs, in contrast to β -tubulin, which has an exchangeable site where the GDP (guanine diphosphate) can be displaced by GTP. Longitudinal contacts between heterodimeric subunits link the subunits head to tail into a straight column, termed as a protofilament. Lateral connections are responsible for side by side association of protofilaments into a cylindrical form (Fig. 6.4). Usually a singlet microtubule is built from 13 protofilaments.

Like an actin filament, a microtubule shows polarity in its structure through head to tail arrangement whereby assembly and disassembly preferentially occur at the plus-end. The stability of a microtubule is strongly dependent on temperature and concentration. Like in the case of actin, there exists

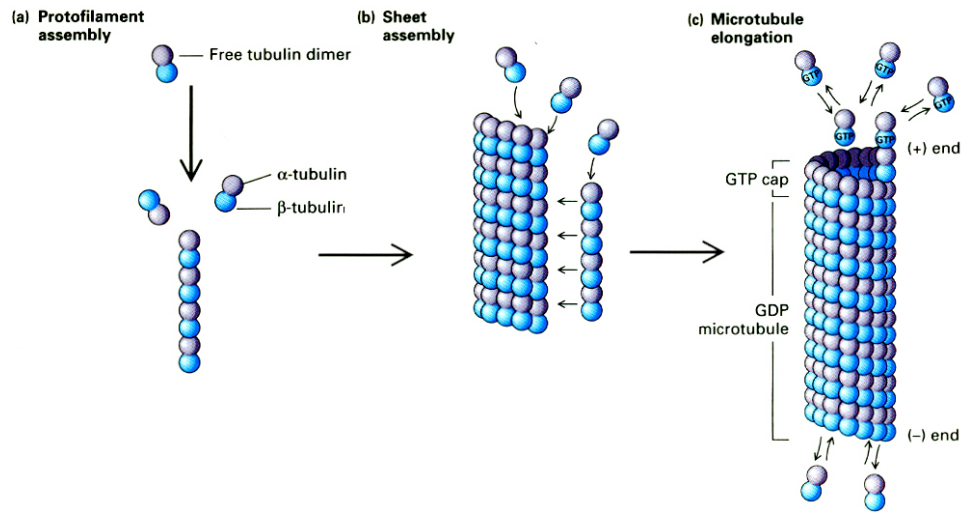


Figure 6.4: Assembly of microtubules: Heterodimeric tubulin subunits add assemble into protofilaments. These protofilaments build sheet-like structures, resulting in cylindrical microtubules. From ref. [18].

also a critical concentration for tubulin. At tubulin concentrations above the critical concentration, microtubules polymerize, while at concentrations below the c_{crit} , depolymerization occurs. Microtubules can grow while simultaneously other nearby microtubules shrink. Also a single microtubule can oscillate between growth and shortening phases. The specific factors that switch a microtubule between growth and shortening are not understood.

6.2.2 Microtubule-Organizing Centers and Associated Proteins

Microtubule-organizing centers play the central role in nucleating the assembly of new microtubules [45]. In most animal cells they contain a pair of orthogonally oriented centrioles at the center of the amorphous cytosol. All

microtubule-organizing centers contain γ -tubulin, a non-polymerizing isotope, which serves as a nucleus for $\alpha\beta$ -microtubules polymerization [45]. The slow growing minus-end is oriented towards the microtubule-organizing centers, whereas the plus-end points towards the front of the cell.

Microtubule associated proteins are responsible for cross-linking microtubules into bundles. They are organized in two domains, a microtubule-binding domain and an acidic projection domain. The projection domain is able to bind to membrane, intermediate filaments, or microtubules. Its length determines the spacing between microtubules in a bundle. The microtubule associated proteins also stabilize microtubules by coating their outer wall, preventing tubulin subunits from dissociating.

6.2.3 Motor Proteins

Microtubule motor proteins bind to microtubule in presence of ATP whereby the actual movement requires hydrolysis of the bound ATP. Transport in both directions along one single microtubule is possible. Anterograde conveyance represents transport in the direction away from the cell body whereas retrograde transport goes towards the cell body. Two molecular motor proteins, which are responsible for axonal transport in neurons and vesicle movements in other cells, have emerged. Kinesin (MW 380000 u) is a plus-end directed motor protein and is responsible for anterograde transport whereas dynein (MW > 1000000 u) powers movement in the opposite direction, towards the minus-end.

6.3 Intermediate Filaments

Intermediate filaments are present in nearly all eukaryotic cells. They are organized in the cytosol in a pattern similar to that of microtubules. Intermediate filaments provide mechanical support to the plasma membrane where it comes in contact with other cells or the extracellular matrix. Therefore its function is mainly of structural nature. They are not involved in generating any movements. Intermediate filaments are extremely stable, compared to actin filaments or microtubules [18]. They are rope-like polymers, composed of α -helical subunits. Intermediate filaments do not bind nucleotide, such as ATP or GTP, and its polymerization process does not require hydrolysis, in contrast to actin and microtubules assembly.

Intermediate filaments are classified into five main classes, e.g., keratins, vimentin, or lamin. Each class of proteins is characteristic for a certain tissue or cell type, such as vimentin is typically found in fibroblasts. All intermediate filament subunit proteins are similarly organized in three domains, a central α -helical core and contiguous globular N- and C-terminal domains. The α -helical segments pair to form a coiled coil dimer, which appears as a rodlike molecule with globular domains at the ends. The dimers associate laterally (antiparallel) into a tetramer with a length of 70 nm. Tetramers bind end to end, forming protofilaments (2 nm thick), which pair together into 4 nm-thick protofibrils. Finally, four fibrils form a single intermediate filament that is 10 nm in diameter. Intermediate filament subunits are able to associate to, and dissociate from existing filaments.

The intermediate filaments are cross-linked into a bundle, a network, or to the plasma membrane by intermediate filament associated proteins. Plectin, for example, is able to bind to intermediate filaments and microtubules and it is also known to interact with other cytoskeletal proteins. Therefore, a possible role of intermediate filament associated proteins is to connect intermediate filaments to the microfilament and microtubule cytoskeleton [18].

Consistent with the fact that intermediate filaments are not actively involved in motility processes, there is no intermediate filament related motor protein known. There is also no evidence of any capping, severing, or sequestering proteins.

Chapter 7

Cell Lines

7.1 Basics of Cell Motility

In Chapter 6 we already examined different mechanisms used by a cell to create movements. These include the assembly of actin filaments and microtubules, formation of bundles and networks, and sliding of single motor proteins, such as myosin and kinesin, along actin filaments or microtubules. In general, the changes in cell morphology of a moving cell can be classified in three sequenced phases: protrusion, traction, and retraction (see Fig. 7.1). Protrusive structures at the leading edge of motile cells are highly dynamic and contain dense arrays of actin filaments. A simple protrusive structure are filopodia (actin bundles), which can extend tens of microns from the main cortex. Lamellipodia are thin protrusive sheets that dominate the leading edge in many motile cells, such as cultured fibroblasts, keratocytes, and growth cones. The web that shapes lamellipodia is composed as an orthogonal network of two sets of filaments oriented at approximately 45° to the direction of protrusion [26, 46]. Attachment to the substratum anchors the cell and prevents the leading lamella from retracting. Conversion of protrusion into movement along the substrate is consequently possible. Cells can either form focal contacts or close contacts, whereby the force exerted to the substratum

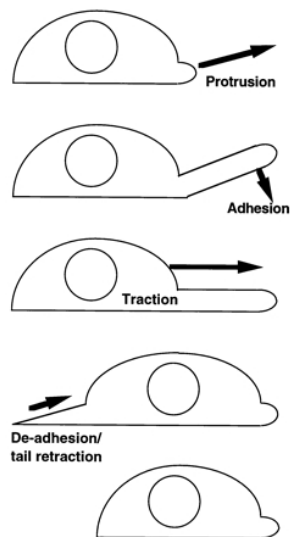


Figure 7.1: Three coordinated motility steps: Protrusion and adhesion of the front end occurs, which is here shown as two individual steps, followed by traction that leads to the advance of the nucleus. Finally, release and retraction of the tail happens. Detailed morphology varies between cell types, but the same basic steps in motility can be distinguished. From ref. [46].

by focal contacts is 10-100 times stronger than by close contacts [43, 27]. The process leading to forward movement of nucleus and bulk cytoplasm is termed traction. It is maybe the most important step in cell motility but also not very well understood. The last step in locomotion is retraction of the tail. Here, the tail deadheres from the substrate and snaps forward. Neuronal growth cones lack this tail retraction. Nevertheless, deadhesion still occurs, since the axon is more weakly substrate bound than the front of the growth cones [13, 46].

Concerning our experiment, where we try to influence the cell's leading edge to protrude into the laser beam, we want to have a closer look at the extension step and possible forces for cell protrusion. Here, I will focus mainly on the actin cytoskeleton, which is believed to be the basic engine for crawling or gliding locomotion [46]. Microtubules are important for polarity and also motility, but compared to actin, they may usually play only a sec-

ondary role. In any case, protrusion of the membrane is strongly coupled to actin polymerization at the leading edge, which occurs continually at steady state (treadmilling). To provide and incorporate new actin monomers at the cell's front depolymerization elsewhere is necessary. It is widely accepted that the force for protrusion is locally generated at the leading edge. Fig. 7.1a

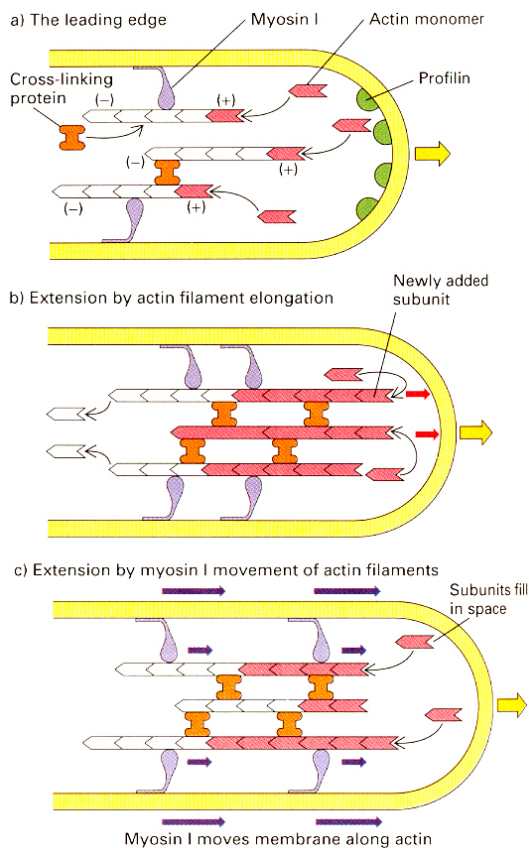


Figure 7.2: Force for protrusion: a) Sketch of leading edge with polymerizing actin; actin cross-linking proteins stabilize actin filaments into bundles and networks; myosin I is thought to be connected to the plasma membrane; b) Actin filaments elongate at the leading edge under addition of subunits which push against the cell membrane. c) If actin filaments are connected to other cytoskeletal structures, then myosin I can walk along these filaments and extend the cell membrane. The resulting space can be filled by newly polymerized actin. From ref. [18].

shows a cartoon of the leading edge, containing actin filaments and several proteins, such as profilin and myosin I. The actin filaments are oriented with their barbed ends towards the cells edge. Several mechanisms for generating

the force for protrusion have been proposed. The membrane may be extended forward just by the pushing action of the polymerizing actin filaments [18, 23], shown in Fig. 7.1b. In addition, the "Brownian ratchet" model is a simple explanation for membrane protrusion in which either the plasma membrane or the actin filaments at the leading edge fluctuate as a result of Brownian motion. Its outward excursions provide space for actin subunits to add to actin filaments at the membrane-cytoplasm interface [23, 49]. Another model involves myosin I, an actin motor protein. Myosin I connected to the plasma membrane moves forward along actin filaments and clears space for the addition of actin monomers to the ends of the elongating filaments [18] (Fig. 7.1c). The requirement therefore is, that the actin filaments are positioned to other cytoskeletal fibres. A combination of all effects is also conceivable. Similar mechanisms, involving tubulin polymerization and microtubule motor proteins, like kinesin, are considered but not very extensively studied. Note, that this are all hypothesis, which are not proven yet and need to be resolved.

7.2 Fibroblasts

Cultured fibroblast (Fig.7.3) have the morphology of tissue fibroblast, but they retain the ability to differentiate into other cell types. We used two cell lines of fibroblast, BALB/3T3 and SV-T2 (both from ATCC). These cell lines, developed by S. A. Aaronson and G. T. Todara, stem from 14- to 17-day old BALB/c mouse embryos (*mus musculus*) [39]. The SV-T2 cells are derived from BALB/3T3 and transformed by the oncogenic DNA virus SV40.

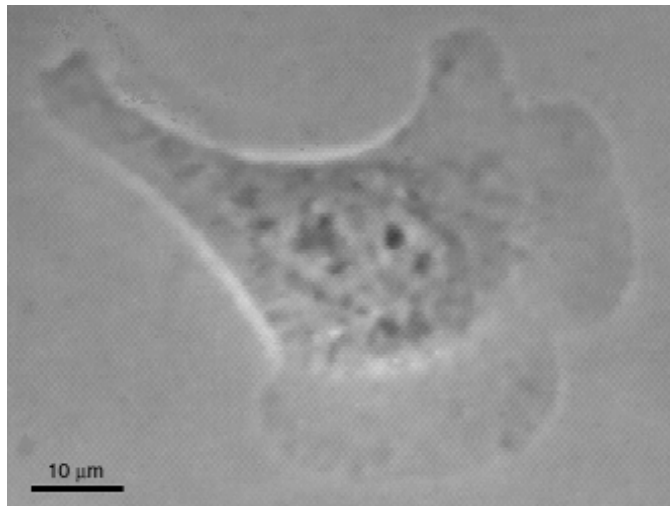


Figure 7.3: Cultured SV-T2 cell crawling downwards to the right. One can see the nicely spread lamellipodium and on the opposite side the tail of the cell.

Fibroblasts are counted among the classic models of cell motility and many studies of cytoskeletal organization and dynamics have been carried out in this system.

7.2.1 Fibroblast Locomotion

Cultured fibroblasts flatten onto the surface and crawl over the substratum. In the body, this property of crawling is rarely seen, usually only in the course of wound healing. Fibroblasts are normally static cells that secrete and maintain the collagen-rich extracellular matrix [14]. Fibroblasts are slow moving cells, advancing and pausing at irregular intervals. They have the ability to adhere tightly to the substratum and pull against it. Cortical actin gathers in adhesion plaques that pin the fibroblast down to the substratum.

These adhesion plaques oppose the contraction of the cortex and distinct actin filament bundles (stress fibers) are formed (Fig. 7.4). Otherwise the cell would become round [14, 4]. Only lamellae that contact the substratum on which the cells are crawling can generate locomotion. For fibroblasts, it has been directly shown that actin filament polarity is uniformly with barbed end forward [31], supporting a treadmilling model, where protrusion involves addition of new actin subunits at the leading edge (see § 7.1). Furthermore, protruding fibroblasts show a phenomenon, called ruffling, in which the leading edge of the lamellipodium lifts upward from the substratum and, while continuing to protrude, bends backward [49]. This is illustrated in Fig. 7.4. The ruffle mi-

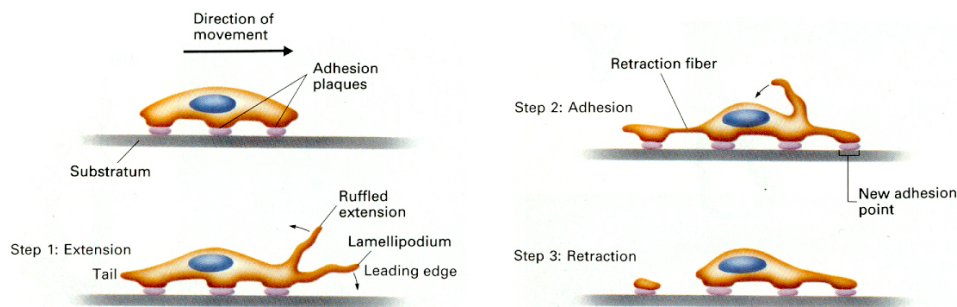


Figure 7.4: Fibroblast locomotion: Cell attaches to substratum and builds adhesion plaques. Step 1: Fibroblast protrudes forward in addition to ruffling. Step 2: Cell adheres and moves cell body forward. Step 3: Fibroblast retracts tail, whereby often leaving a bit of strongly adhered membrane. From ref.[18].

grates rearward and collapses in a wave-like manner near the cell body. After forming a new adhesion point, the cell body moves forward. Inherently, the traction force seems to be stronger than the protrusion force and is therefore probably more important for cells that are strongly attached to the substrate,

e.g., fibroblasts. One hypothesis for the traction force is that the nucleus and the other organelles are embedded in the cytoskeleton and that the whole cytoskeletal framework is pushed or pulled forward [18]. This process may be driven by myosin II which is known to be abundant in the cell body. There is evidence either for contractile models [14], where force is generated as tension, or for transportational models, where the cell is pulled forward. So far, detailed understanding of the traction force in fibroblasts is missing. In the last step of movement, the tail snaps loose from its connections and is brought forward. In this retraction step, usually a little bit of the fibroblasts membrane is left behind because of its strong adhesion to the substratum (Fig. 7.4).

7.2.2 Cell Culture

BALB/3T3 and SV-T2 cells are treated identically. Exchange of medium (90 % DMEM, 10 % CS, 10 mM HEPES, 10 ml antibiotic solution), called feeding, is usually done every 3 days. Passaging and plating is done every 7 to 10 days, as described in Appendix D.2.

In order to enhance the activity of the fibroblasts during the experiment, the cells (on sample dish) are feeded with recombinant rat platelet-derived growth factor-BB (PDGF-BB from Sigma) drugged medium at least 36 hours in advance. Moreover we try to grow the fibroblast not too dense on an experimental dish to achieve observation of individual moving cells. The SV-T2 cells seem to be a bit more motile and active than the BALB/3T3 cells when treated with the PDGF-BB.

7.3 Keratocytes

The fish keratocyte (Fig. 7.5) is an epithelial cell, which was first described by Goodrich (1924) [19]. Keratocytes of four different fish types (Goldfish, Silver Molly, Dalmatian Molly, and Black-Skirt Tetra) are used. Keratocytes are comfortable in a relatively broad range of temperatures, e.g., goldfish keratocytes are fine between 8–30 °C. In contrast to fibroblasts, fish epidermal keratocytes have a simpler shape and pattern of movement. Therefore this cell type is very common for studies of cell locomotion.

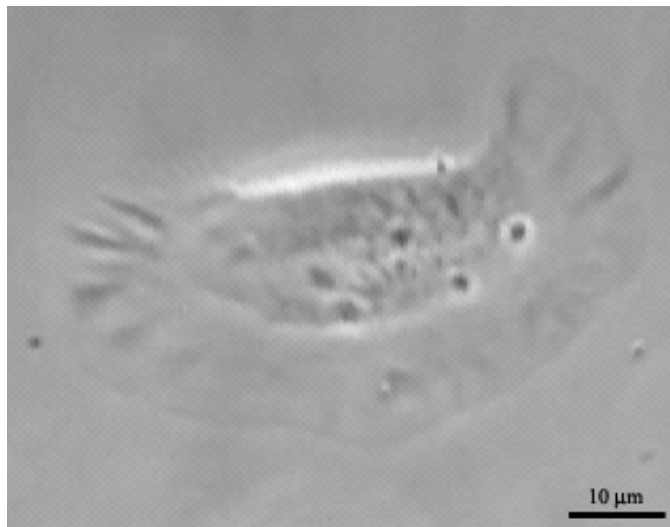


Figure 7.5: Goldfish keratocyte with fan-like spread lamellipodium. Direction of movement of cell is perpendicular to the long axis of the cell.

7.3.1 Keratocyte Locomotion

Fish keratocytes are wing-shaped cells, referred by Goodrich as "canoe cells", with a large lamellipodium filled with actin (Fig. 7.5). During keratocyte movement, which is smooth and continuous, the cells maintain a constant morphology with well-defined regions. This is thought to be due to nearly perfect coordination among the protrusion, traction, and retraction phases [46, 40]. Keratocytes are fast-moving cells (typically $20 \mu\text{m}/\text{min}$) and their direction of movement is perpendicular to the long axis of the cell [26]. During movement, the actin cytoskeleton stays stationary relative to the substratum, indicating that the rate of actin polymerization equals the rate of protrusion [24, 48]. It was shown by ultrastructural study that a large amount of actin filaments, assembled in a dense network, is abundant in keratocyte lamellipodia. Here, the actin filament polarity is uniform, with fast growing ends forward. As for the fibroblasts, this might be a supportive indication for a treadmilling model of the leading edge protrusion [48]. Microtubules were mostly found near the cell body and they were not localized in the lamellipodium, suggesting that this fibril does not directly affect protrusion of the leading edge [48].

Although in freely locomoting keratocytes, protrusion and traction seems to be tightly coupled, which results in a stable cell shape, there is evidence that their mechanisms are independent [28, 48]. It is proposed that myosin II, which is highly distributed in the lamellipodia-cell body transition zone, interacts with actin by "dynamic network contraction" [48]. The

actomyosin-based contraction pulls the cell body forward and causes the actin network to collapse into bundles at the transition zone (Fig. 7.6b,c). This

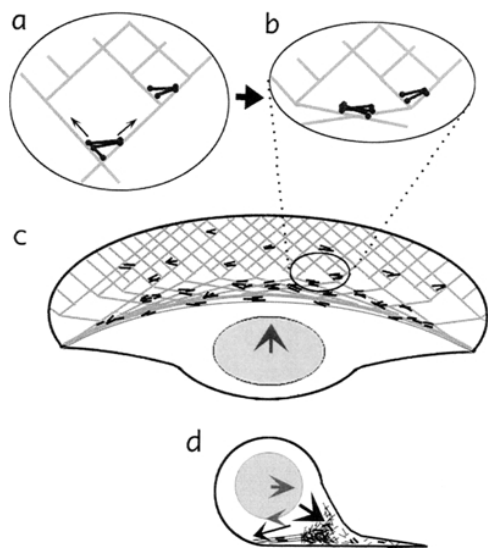


Figure 7.6: Dynamic network contraction: (a) Actin network (light grey lines) and myosin (dark bipolar filaments) in the lamellipodium of a keratocyte. (b) Myosin clusters move forward and actin is brought into alignment as parallel bundles. (c) Network contraction causes forward translocation of the cell body. (d) Cross-section view, where forward rolling of the cell body is shown. From ref. [48].

concentration of cytoskeletal filaments near the bottom of the cell creates a drag force. That, in combination with the forward translocation force, causes the cell body to rotate (Fig. 7.6d) and to be pulled forward [40, 48].

Fast moving cells, such as keratocytes or neutrophils, form weaker close contacts with the substrate, whereas slower moving cells, such as fibroblasts, form stronger focal adhesions. This suggests that slower moving cells may be hindered in their motility by their strong contacts [27, 43]. During the traction-retraction step, keratocytes usually do not leave cytoplasmic trails, in contrast to fibroblasts.

Chapter 8

In vivo Experiment

8.1 Setup

The setup we use in the experiments with fibroblasts and keratocytes is the same setup which is used in the neuronal growth cone guiding experiments. The laser system consists of a Millennia V8 (Spectra Physics), used as pump-laser, and a Kapteyn Murnane Ti:Sapphire, both pictured in Fig. 8.1. The

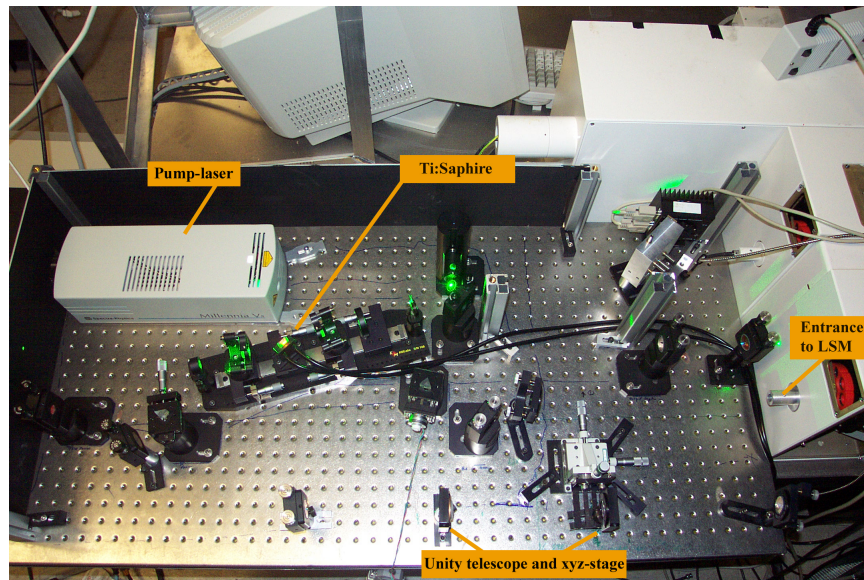


Figure 8.1: Laser system and beam path: The Millennia (pump-laser) pumps the Ti:Sapphire. The laser beam goes through a 1 : 1 telescope on an XYZ-stage and enters the LSM.

threshold pump power is ~ 2 W. At the maximum pump power of 5.5 W, we measure ≈ 1.25 W at 800 nm at the entrance to the Zeiss model LSM 410 invert (Laser Scan Microscope). The laser beam passes through the laser

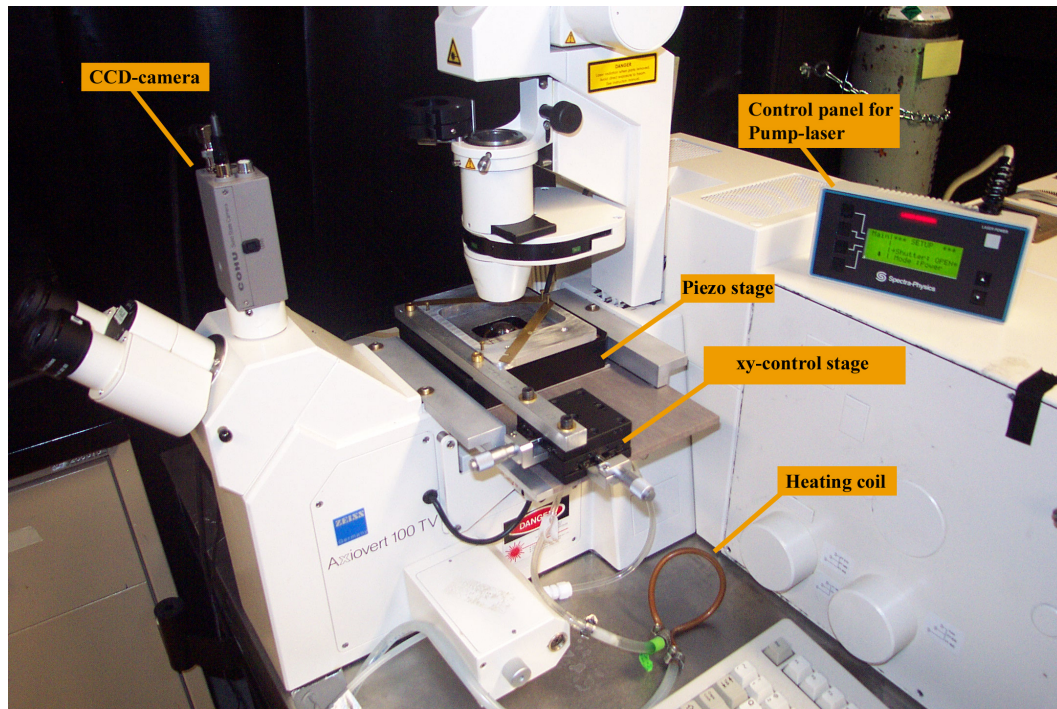


Figure 8.2: Setup for experiments on fibroblasts and keratocytes. The sample dish is placed and fixed on the piezo stage. A copper coil is used for regulating the sample temperature to 37 °C. Imaging of the cells is performed with a CCD-camera.

port and mirror system of the LSM and enters the Zeiss Axiovert 100 TV microscope, where it is reflected from a dichroic mirror in a filter cube located underneath the microscope revolver. The beam then travels through a $63\times$ oil objective (Zeiss Plan Neofluor, Ph3, $NA = 1.25$) and is focused in the sample plane with a spot size of ~ 2 μm . The beam loses about 80 – 90 % of its

power in this optical path, which results in a maximum power of ≈ 140 mW after the objective. The losses are due to reflection and absorption in the internal lens system of the LSM and the absorption in the $63\times$ objective. In our experiments, we usually use a power of ~ 100 mW. The laser beam was centered via an XYZ-stage, pictured in Fig. 8.1. A nearly 1 : 1 enlargement telescope is used to control the divergence of the laser beam before the $63\times$ objective.

The objective and the sample dish are heated with resistive copper coils, whereby a constant temperature of 37 °C is achieved. The dish is clipped to the microscope stage (Fig. 8.2), which consists of a piezo-driven XY stage (Physik Instrumente) embedded in a teflon-coated aluminum stage with XY-control. To achieve optical guidance, the beam is interactively steered by the LSM or by moving the microscope stage relative to the laser beam with the piezo-driven XY stage. The piezo-driven stage is computer controlled, so that scan width, scan speed, and angle can be selected. It is only used for scanning experiments, whereas the XY-control of the aluminum stage is used in the process of searching for active and motile cells.

Phase-3 contrast imaging is done with the Axiovert microscope. For documentation, a CoHu CCD-camera is connected to the microscope either through the lower port, resulting in a $\approx 42 \mu\text{m} \times 32 \mu\text{m}$ field of view, or through the upper port with a $\approx 121 \mu\text{m} \times 91 \mu\text{m}$ field of view. The CCD signal is recorded on videotape by a VCR.

8.2 Sample Preparation

The fibroblasts in the experiments are plated on sample dishes (see Appendix D.2). Shortly before the experiment, the inner petri dish of a sample dish (Fig. 8.3) is filled with fibroblast medium until there is a convex meniscus (≈ 27 ml). The lid (which has a small hole in the top) is sealed to the dish around the edges with high vacuum grease (Dow Corning), to reduce penetration of bacteria. The space between the two compartments of the

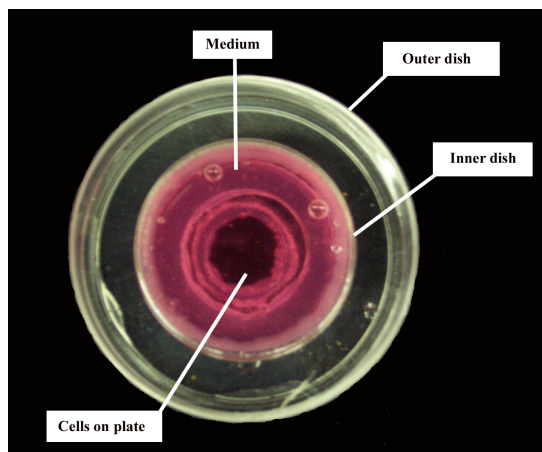


Figure 8.3: Sample dish. The dish consists of two compartments, an inner and outer dish. The cells are plated on the inner dish (dark spot). Water is filled in the space between the inner and the outer dishes. The heating coil is placed around the inner dish.

sample dish is filled halfway with distilled water. A copper coil (Fig. 8.2) is placed inside the water to heat the sample uniformly.

The keratocytes are also cultured in sample dishes. Before a cell-containing dish is used in an experiment, it is rinsed with 1 ml PBS, followed by the addition of 1 ml of medium. Heating of the objective, sample, and medium are not necessary because keratocytes are comfortable at lower temperatures.

8.3 Procedure and Results

An experiment begins when the heating system is turned on, since it needs about 45 minutes to warm the copper coils to the desired temperature. Then the chiller of the pumping laser is turned on, followed 10 minutes later by the turn-on procedure of the pumping laser itself. The computer and the LSM are booted up and the 63 \times objective is cleaned with lens tissue. Measurements of the actual laser power after the 63 \times objective are done with a Coherent power meter with pump powers ranging from 3 W to 5.5 W, with increments of 0.5 W. The numbers are plotted with Microsoft Excel to determine the laser output power as a function of pump power. Before getting the sample ready (§ 8.2), the piezo-stage, VCR, and TV are also turned on.

The objective is cleaned again before putting a drop of immersion oil on it. Next, the sample dish is fixed to the stage and the cells are observed with the Axiovert microscope. With the help of the XY-control stage, single active cells are identified. Then, the beam path to the CCD-camera is opened and the signal recorded. In the case of fibroblasts, we observe the cell activity and behavior for about 10 – 20 minutes without laser light (for keratocytes only 2 – 3 min). Then the laser beam is unblocked and interactively steered with the confocal scanning microscope to the leading edge of the cell. The actual line scanning with the desired scan properties is activated by the computer programm. The sample on the piezo-driven stage is moved relative to the objective and thus to the laser beam.

The recorded videotapes of interest are grabbed by the program scion

image with the aid of a VCR, connected to a computer. Single pictures or whole sequences can be transferred to the computer. The pictures are cleaned up with Photoshop 5.5.

We started our experiments with fibroblasts which were not active or mobile, and we did not observe any reaction to the laser. In the body, fibroblasts are active in the process of wound healing. Thus, we simulated this situation by growing them confluent and starving them with serum free medium. Additionally, a scratch (40 – 80 μm in width) through the dense network of cells was made with a micropipette. The gap was closed by the fibroblasts but more by contraction, once they were connected to both sides, than by crawling into the gap. It was impossible to start an experiment with defined conditions. Hereupon, we treated the fibroblasts with PDGF-BB and used an additional, more active cell type: fish epidermal keratocytes.

Fig. 8.4 shows a series of four pictures, representing a typical experiment. In this experiment, we observed an active and motile cell. Shortly before we started to exert influence on the sample with the laser, the cell looked like to be in a resting phase. Immediately after turning on the laser, the lamellipodium of the fibroblast seemed to extend and to level off in the scanning area. Nevertheless, the rate of extension was not recognizable higher as it was before, when the cell was in an active phase, uninfluenced by the laser.

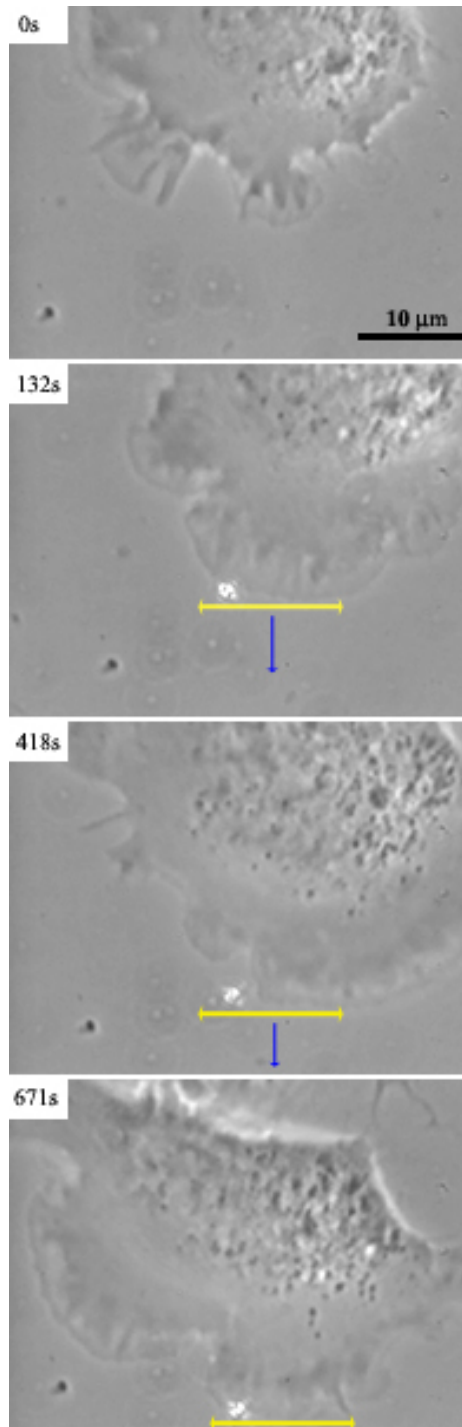


Figure 8.4: Experiment with PDGF-BB treated SV-T2 cells with 100 mW beam power: The yellow line below the laser spot (bright spot) represents the scanning width, which is $15\ \mu\text{m}$ in this case. The scanning speed was $2.75\ \mu\text{m/s}$. The blue arrow shows the direction of guiding. In the upper left corners, the time in seconds is given. The first picture shows the cells leading edge immediately before the laser was pointed at it. The successive pictures show the cells response at different times. After about 2 minutes the leading edge already flattened out and showed a nice lamellipodium. After another 4.5 minutes the leading edge moved further downward as did the whole cell. The cell moves down and to the left side as can be seen in the last picture (another 4 minutes later). The lamellipodium in the laser scanning region almost seems to match the scan width and builds a straight line. The pictures were taken with phase 3 contrast microscopy.

Fig. 8.5 shows pictures of another experiment on fibroblasts. In this case the fibroblast crawled downwards and towards the right side. The activity of the leading edge towards these directions was favored. As soon as we turned on the laser, the front of the cell oriented itself more downward. During the first 21 minutes the tail of the cell partially retracted and brought the cell forward, which can be seen in the second picture. After another 30 minutes, the left side of the cells leading edge reached a nice extension. The laser beam was not always pointed on the leading edge. Levelling over the scan width was aimed at, but did only partially succeed (picture at 21 minutes). The left side of the cells front was always more active and extended even when the laser was not all along right at the leading edge.

Unfortunately, we do not have enough material to do statistics. We did about 13 reasonable experiments where the cells were active and motile. We can say so far, that the laser light has an influence on the fibroblasts, even though it is very little. Guiding of a whole fibroblast was not achieved. In many experiments, we saw parts of the leading edge extending and following the beam path. In the majority of cases this was only seen briefly and over short distances. Also, in most experiments on the fibroblasts a dark line appeared temporarily in the lamellipodium where the laser was scanning, indicating that this region is thicker than its surrounding area. A significant increased extension rate of lamellipodia was not observed. Admittedly, lamellipodia of the fibroblasts did not always follow the laser beam (3 experiments). Retractions were never observed.

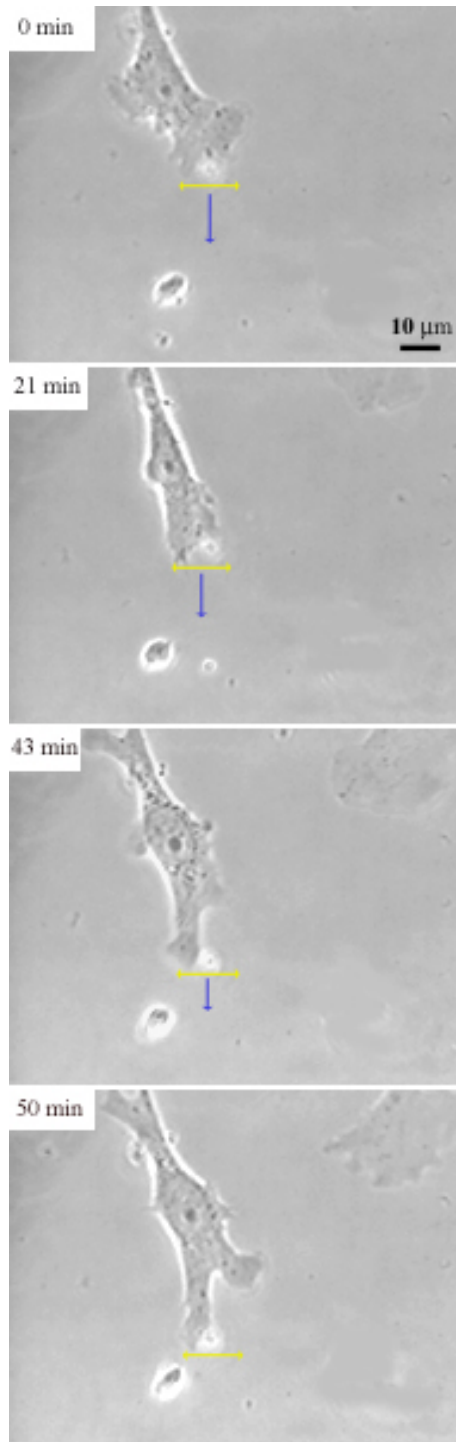


Figure 8.5: Another experiment with PDGF-BB treated SV-T2 cells with 100 mW laser power: The yellow line below the laser spot (bright spot) represents the scanning width, which is $15 \mu\text{m}$ in this case. The scanning speed was $2.75 \mu\text{m/s}$. The blue arrow shows the direction of guiding. In the upper left corners, the time in minutes is given. On the first picture one can see the cells leading edge at the moment when the laser was placed at the cells front. The cell was heading down to the right side at this moment. The next picture shows the cell after 21 minutes. During this time the cell crawled more downward and its front width matches about the scan width. After another 22 minutes the cell itself stays almost at the same place but the leading edge is extending to about $15 \mu\text{m}$. The scan width does not match the cell width any more. 7 minutes later the leading edge is still extending to about another $8 \mu\text{m}$. The pictures were taken with phase 3 contrast microscopy.

Fig. 8.6 illustrates an experiment with a keratocyte of a dalmation molly. In the first picture, the keratocyte is heading to the right and somewhat upwards. It lacks some of the lamellipodium in the lower region. We scan with the laser over a region of $13\ \mu\text{m}$ in a 45° angle. After $42\ \text{s}$ the lamellipodium has already grown into the scanning region. After almost $2\ \text{min}$ the lamellipodium extension on the lower side is bigger than elsewhere. The cell changes its direction of movement, as can be seen in the upper right picture ($228\ \text{s}$). After nearly $6\ \text{min}$ the laser scanning is stopped to change the scan angle. In the period between $354\ \text{s}$ and $607\ \text{s}$ laser scanning is done first in a 30° angle (not pictured) and then horizontal (last picture). In the meanwhile the cell turned, but did not stop to turn, even as we tried to guide it downwards. Unfortunately this experiment was rather an exception. In nearly all 15 experiments on the keratocytes we did not see a recognizable effect, except for the appearance of a dark line in the lamellipodium in the scanning region of the laser, which also occurred in case of the fibroblasts. We will try to investigate this phenomenon in the future.

For comparison only, Fig. 8.3 illustrates two optically induced turn experiments of PC-12 neurons. The left picture series shows a turn of a large growth cone. Here the turn takes a longer time period than in the case of a smaller growth cone, see picture series on the right. The extension rate of the larger growth cone was slower than in the smaller growth cone. Note that the lamellipodia of growth cones do usually not cover a large region, which is especially shown in the right picture series.

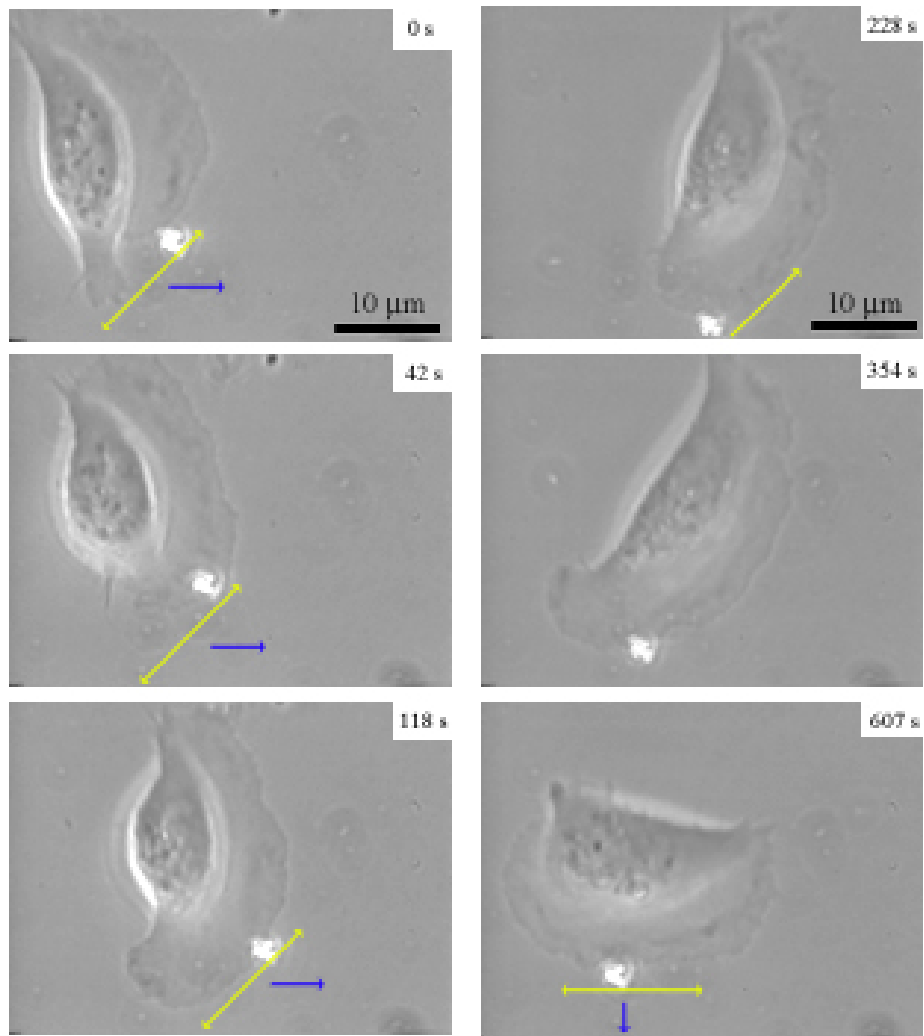


Figure 8.6: Experiment with a keratocyte of a dalmation molly with 82 mW laser power: The yellow line below the laser spot (bright spot) represents the scanning width, which is $13 \mu\text{m}$ in this case. The scanning speed is $3.1 \mu\text{m/s}$. The blue arrow shows the direction of guiding. At 0 s, when the laser is turned on, scanning in a 45° angle, the keratocyte crawls to the right and a little upwards. Shortly afterwards, the lack of lamellipodium in the lower region of the cell is quickly closed (picture 2). The lamellipodium grows out in the laser region (picture 3) and the keratocyte changes the direction of movement (pictures 4 – 6). After ≈ 400 s the cell crawled out of the field of view, so we had to move the sample with the xy-control of the microscope stage. Therefore the last picture is not taken on the same spot as the five before.

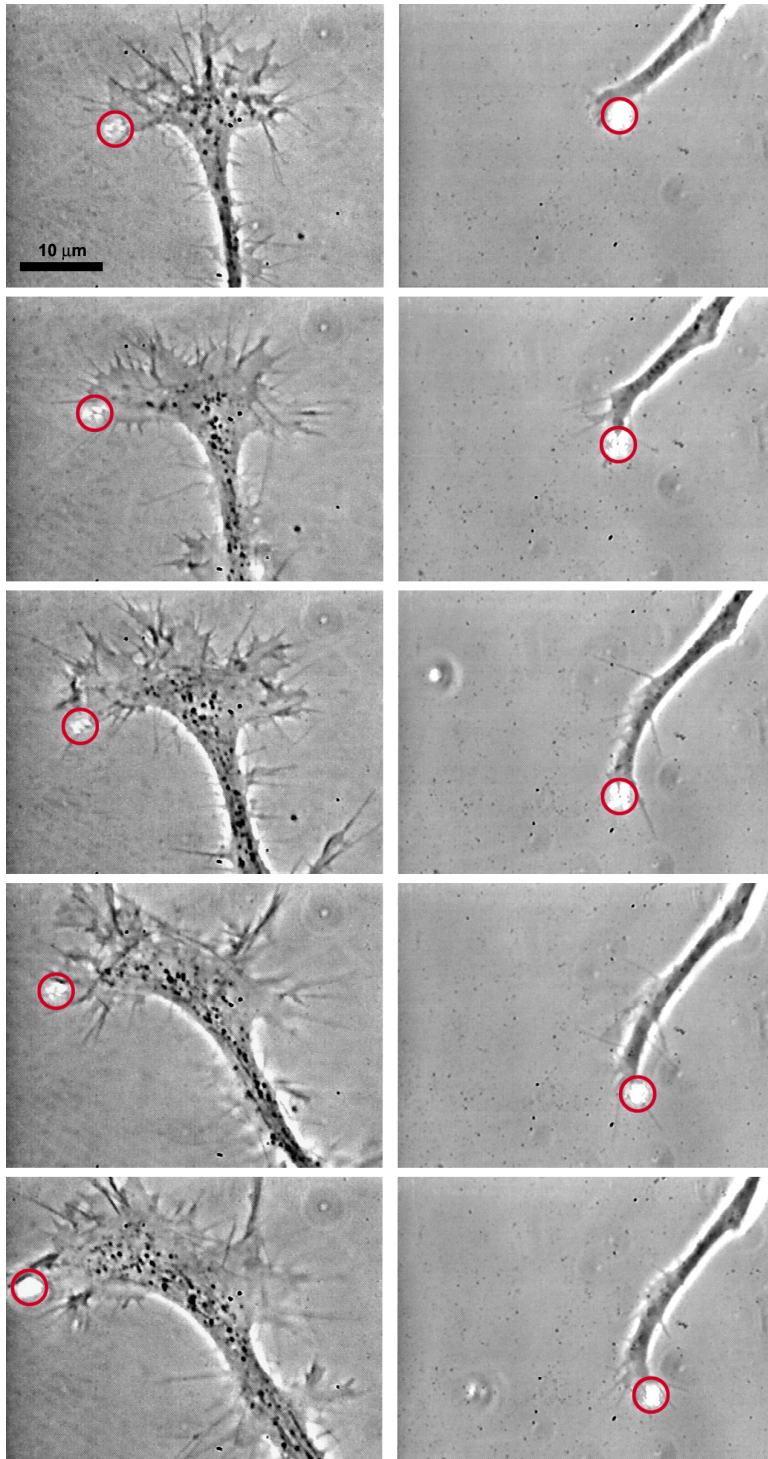


Figure 8.7: Experiment with PC-12 neurons: Optically induced turns of PC-12 neurons. In each sequence the red circle marks the laser spot.

Left: 40 min time period, 10 min between successive pictures, 100 mW laser power;

Right: 20 min time period, 5 min between successive pictures, 60 mW laser power. From ref. [15].

Chapter 9

Conclusion and Outlook

Overall, the results to the experiments on the three cell types, i.e. neuronal growth cones, fibroblasts, and keratocytes, may match into a model of biased actin polymerization. Growth cones are slow moving cells with a relatively small area of lamellipodia at the front of the cell. Achievement of guidance of the growth cones might be due to these two properties. Fibroblasts are also slow crawling cells but they are bigger and show a larger region of lamellipodia at the cell's front. We can state, that there is an effect of the laser on the PDGF-BB treated fibroblasts. Nevertheless, the results are not significant enough and we are far away from fibroblast guiding. Keratocytes, a fast moving cell type, show well defined, relatively large, wing shaped lamellipodia. In the experiments on these cells, no significant effect is observed. There is a possibility, that keratocytes are just too fast to respond to the laser. Therefore, the actin flux into the laser spot would be too slow, which is confirmed by drift velocity calculations. The drift velocities are on the order of a few tens of micrometers per hour (§ 4.2 and ref.[1]), whereas a keratocyte can move with velocities up to a few tens of micrometers per minute [48]. This criterion of the drift velocity of actin also matches the observations on the two slow moving cell types. In case of the fibroblasts, the size of the cell

and its lamellipodia might be the reason why guiding could not be achieved, in contrast to the neurons. Here, a more powerful laser could play an important role, when scanning over a larger region of the lamellipodium. This will be studied on a new setup, where an external fiber laser will penetrate the sample from the top. Thus absorption losses in the microscope and objective will be bypassed. Even if the experiments with the keratocytes were not successful so far, we will also continue with this cell line in the future. We plan to cool the sample from room temperature to 10 °C in order to slow the keratocytes down. Using more sticky substrates is also a common method to decelerate cells. With that, it is conceivable that the laser affects the cell because actin monomers have more time to drift into the beam spot. Besides, the effect of a more powerful laser would also be interesting.

Due to the fact that optical guiding of keratocytes and fibroblasts is not successful so far indicates that the responsible mechanism for neuronal growth cone guiding is not based on a temperature effect, where the laser spot heats the sample locally.

Further possibilities for studying cell systems and the role of actin are fluorescence experiments on actin monomers. Even simultaneous observation of monomeric and filamentous actin under the influence of a laser beam can be done. For this, Fluorescein DNase I (D-970) can be used in combination with fluorescently labelled phallotoxins. Indeed, observation of the small actin concentration increase (see § 4.3) at the cells front seems to be rather implausible.

Other cell types, such as neutrophils, can be tested and their response may give additional information, why guiding works on one type of a cell but not on another. Neutrophils might be suitable because they are small and active.

If it emerges that fibroblast guiding works, there might be some applications in the process of wound healing. It would be feasible that growth of fibroblasts or other tissue cells are enhanced by the laser light, which might result in an accelerated closure of a wound.

Appendices

Appendix A

Actin Sample Preparation

- ***Antibleach***

- * Put 1.35 ml of distilled H₂O in a 1.5 ml Eppendorf tube.
- * Add 150 μ l of F-Buffer (100 mM Tris pH 7.5, 5 mM ATP, 1.5 M KCl, 20 mM MgCl₂, 2 mM CaCl₂).
- * Put a spatula tip of glucose to it and mix it well.
- * Take sample under the hood and add 7.5 μ l of the poisonous BME (Bi-Mercapto-Ethanol).
- * Put a spatula tip of glucose-oxidase in the sample; mix it well and cool it in ice.

As a general rule of thumb antibleach contains about 90 % H₂O, 10 % F-Buffer and 0.5 *vol%* of BME.

- ***Labelling of actin***

- * Put 64.7 μ l of distilled H₂O in a 1.5 ml Eppendorf tube.
- * Add 10 μ l of F-Buffer and mix it.
- * Put 25.3 μ l of G-actin (3.96 mg/ml) in the tube and mix it.
- * Use dim light to add 1 μ l of TRITC-Phalloidin to label the actin filaments.

Appendix B

List of Chemicals

Abbr.	Name	Purpose	Vendor
DMEM	Dulbecco's modified Eagles medium	Main ingredient for fibroblast and keratocyte medium	ATCC
CS	Calf Serum	Ingredient for fibroblast medium	ATCC
FBS	Fetal Bovine Serum	Ingredient for keratocyte medium	ATCC
Hepes		Ingredient for fibroblast and keratocyte medium	ATCC
PBS	Phosphate-buffered saline	Rinsing fluid	home-made
Antibiotic solution, containing 5,000 units/ml of penicilin and 5 mg/ml of streptomycin		Broad spectrum antibiotics against bacterial growth	Sigma
PDGF-BB	Platelet Derived Growth Factor-BB Rat, Recombinant	Activity enhancement of Fibroblast	Sigma
TRED	Trypsin/EDTA	Deadhesion of cells from substrate	ATTC
Laminin (1 mg/ml)		Enhancement of cell adhesion	Sigma
DMSO	Dimethyl sulfoxide	Ingredient for freezing medium	Sigma

Table B.1: Chemicals for cell culture

Appendix C

Cell Medium

- **Materials**

- * DMEM
- * CS (fibroblast) or FBS (keratocyte)
- * 10 mM Hepes solution
- * streptomycin
- * 0.22 μm filter
- * Sterile 500 ml glass bottle
- * 50 ml centrifuge tube
- * Disposable pipet (5 ml)
- * pH strip

The fibroblast medium consists of 90 % DMEM, 10 % CS, 10 mM Hepes. Additionally we add antibiotic solution to prevent bacterial growth. The keratocyte medium, we use, consists of 80 % DMEM, 20 % FBS, 10 mM Hepes, and antibiotic solution.

The following procedure describes the method used to obtain 500 ml of fibroblast medium. It is analogous for the keratocyte medium.

- **Procedure**

- * Place DMEM, CS, Hepes, and antibiotic solution in 37 °C water bath for 20 – 30 minutes.
- * Pour 50 ml of DMEM into 50 ml centrifuge tube and label it with solution, date, amount, and initials.
- * Pour 50 ml tube of CS into DMEM bottle.

- * Obtain 10 mM Hepes and put it into DMEM bottle; mix ingredients.
- * Check pH of solution with pH strip; should be between 7.2 – 7.4. If necessary, make adjustments with HCl or NaOH.
- * Attach filter to glass bottle, add connector to filter and attach vacuum tube. Turn on vacuum pump.
- * Pour solution into filter.
- * Remove filter and add 10 ml of antibiotic solution (unfiltered) to existing solution.
- * Cap bottle and label it with all ingredients, date, and initials.

Appendix D

Fibroblast Culture

D.1 Thawing

- *Preparation*

- * Warmed (37 °C) medium
- * 15 ml centrifuge tube
- * 10 ml pipete
- * 1 ml pipettor and sterile tips
- * Set up balance tube for centrifuge
- * Petri dishes

- *Method*

- * Pipete 9 ml of medium into 15 ml centrifuge tube.
- * Remove cells from frozen storage and thaw in water bath by swirling (\approx 60 seconds). Submerge bottom of cryovial only to prevent water from contaminating vial.
- * Add 1 ml of cells to medium in 15 ml centrifuge tube. Rinse cryovial with an additional 1 ml of medium to get residual cells.
- * Balance centrifuge tube and centrifuge for 4 minutes at 800 rpm.
- * Aspirate medium off pellet to remove DMSO.
- * Pipete 11 ml of medium into petri dish. Use 1 ml of medium from dish and redistribute pellet in centrifuge tube.
- * Add redistributed cells to petri dish. Rinse centrifuge tube to get residual cells.
- * Gently rock petri dish back and forth to spread cells homogenously.

- * Label petri dish with name of cells, passage number, date, and initials.
- * Place petri dish into CO₂ incubator.

D.2 Passaging and Plating

Before the actual passaging procedure, the sample dishes are coated with laminin: Mix 40 μ l of laminin with 960 μ l of PBS (40 μ g/ml laminin solution). Put 200 – 250 μ l, or a sufficient amount to cover only the glass cover slip, of this solution on each sample dish before putting the dishes into the incubator. Leave it in there for at least 2 hours (but let it not dry out) before using them.

• *Preparation*

- * Warmed medium, PBS, and TRED (1/3 trypsin, 2/3 EDTA)
- * 15 ml centrifuge tube
- * Laminin coated sample dishes
- * 10 ml pipets
- * 1 ml, 200 μ l, and 20 μ l pipettors and sterile tips
- * Petri dishes

• *Method*

- * Aspirate laminin off the sample dishes.
- * Rinse sample dishes twice with 1ml PBS.
- * Aspirate PBS off each time.
- * Aspirate medium off petri dish.
- * Rinse with 2 – 3 ml PBS to remove TRED inhibitors. Gently rock dish back and forth.
- * Aspirate PBS off.
- * Spray 2 – 3 ml TRED on petri dish, gently tap side of petri dish to dislodge cells and break up clusters. Place dish for a few minutes in incubator, allowing the cells to detach.

- * Add 8–9 ml medium (so it ends up with 11 ml) to inactivate TRED and pool all cells into 15 ml centrifuge tube.
- * Balance centrifuge tube. Centrifuge for 4 minutes at 800 rpm.
- * Aspirate medium off pellet. Redistribute in 1 – 2 ml medium.
- * Put 800 – 1000 μ l of medium in each sample dish.
- * Add 10–40 μ l of redistributed cells and distribute it homogenously.
- * Put 10 ml of medium in petri dish.
- * Add 80 – 200 μ l of redistributed cells. Gently rock dish back and forth.
- * Label all dishes with cell's name, passage number, date, and initials.
- * Put dishes into incubator.

D.3 Freezing

- **Preparation**

- * Warmed medium, PBS, TRED, and DMSO
- * 15 ml centrifuge tube
- * cryovials
- * 10 ml pipets
- * 1 ml and 20 μ l pipettors and sterile tips
- * Set up balance tube for centrifuge
- * Hemacytometer
- * petri dishes

- **Method**

- * Prepare freezing medium (90 % medium, 10 % DMSO); usually prepared 30 min in advance.
- * Aspirate medium off petri dish.
- * Rinse with 2 – 3 ml PBS to remove TRED inhibitors. Gently rock dish back and forth.
- * Aspirate PBS off.
- * Add 2 – 3 ml TRED, gently tap side of petri dish to dislodge cells and break up clusters. Place dish for a few minutes in incubator.

- * Add 8 ml medium to inactivate TRED and pool all cells into 15 ml tube to centrifuge stock solution.
- * Balance centrifuge tube. Centrifuge for 4 minutes at 800 rpm.
- * Aspirate medium off pellet. Redistribute in 1 – 2 ml medium.
- * Do cell count to determine concentrations for freezing ($1 - 2.5 \cdot 10^6$ cells/vial).
- * Aliquot enough stock solution to give desired number of cells.
- * Centrifuge and aspirate off medium. Resuspend in 1 ml freezing medium and transfer to cryovial.
- * Label cryovial with name of cells, passage number, date, and initials.
- * Place cryovials into styrofoam and wrap in paper towels followed by aluminum foil. This serves to insulate the cryovials to attain a slow freeze.
- * Freeze at -85 °C for at least some hours or overnight to two days, before transferring to liquid N₂ storage.

Bibliography

- [1] A. Ehrlicher, T. Betz, B. Stuhmann, D. Koch, V. Milner, M. Raizen, J. Käs. Guiding neuronal growth with light. submitted to PNAS.
- [2] A. Wegner. Head to tail polymerization of actin. *J. Mol. Biol.*, 108:139–150, 1976.
- [3] A. Wegner, J. Engel. Kinetics of the cooperative association of actin to actin filaments. *Biophys. Chem.*, 3:215–225, 1975.
- [4] A.K. Harris, P. Wild, D. Stopak. Silicone Rubber Substrata: A New Wrinkle in the Study of Cell Locomotion. *Science*, 208:177–179, 1980.
- [5] Bart van Zeghbroeck. *Principles of Semiconductor Devices*. Prentice Hall, 2002.
- [6] BRE. <http://projects.bre.co.uk/cool/therm.htm>.
- [7] M.-F. Carrier. Actin: Protein Structure and Filament Dynamics. *The Journal of Biological Chemistry*, 266(1):1–4, January 1991.
- [8] Chroma Technology Corp.
<http://www.chroma.com/data/fsc-index.cfm>.
- [9] C.J. Lumsden and P.A. Dufort. Cellular automaton model of the actin cytoskeleton. *Cell Motility and the Cytoskeleton*, 25:87–104, 1993.
- [10] C.T. Zimmerle and C. Frieden. Effect of Temperature on the Mechanism of Actin Polymerization. *Biochemistry*, 25:6432–38, 1986.
- [11] C.T. Zimmerle and C. Frieden. Effect of pH on the Mechanism of Actin Polymerization. *Biochemistry*, 27:7766–72, 1988.
- [12] Cytoskeleton, Inc.
<http://www.cytoskeleton.com/abactlg.htm>.

- [13] D. Bray. Mechanical tension produced by nerve cells in tissue culture. *J. Cell Sci.*, 37:391–410, 1979.
- [14] D. Bray, J.G. White. Cortical Flow in Animal Cells. *Science*, 239:883–888, 1988.
- [15] D. Koch. Bio-Optical Neuron Guidance. Master’s thesis, The University of Texas at Austin, 2002.
- [16] D. Pantaloni, C. Le Clainche, M.-F. Carrier. Mechanism of Actin-Based Motility. *Science*, 292:1502–06, May 2001.
- [17] D.H. Wachsstock, W.H. Schwarz, and T.D. Pollard. Affinity of α -actinin for actin determines the structure and mechanical properties of actin filament gels. *Biophysical Journal*, 65:205–214, 1993.
- [18] H. Lodish. *Molecular Biology of the Cell*. Scientific American, 1995.
- [19] H.B. Goodrich. Cell behavior in tissue culture. *Biol. Bull. (Woods Hole)*, 46:252–262, 1924.
- [20] J. Käs, H. Strey, J.X. Tang, D. Finger, R. Ezzell, E. Sackmann, and P.A. Janmey. F-Actin, a Model Polymer for Semiflexible Chains in Dilute, Semidilute, and Liquid Crystalline Solutions. *Biophysical Journal*, 70:609–625, 1996.
- [21] J. Käs, J. Guck, D. Humphrey. Dynamics of Single Protein Polymers Visualized by Fluorescence Microscopy. In G. Isenberg, editor, *Modern Optics, Electronics and High Precision Techniques in Cell Biology*, pages 103–137. Springer Verlag, 1997.
- [22] J.A. Barden, M. Miki, B.D. Hambly, C.G. Dos Remedios. Localization of the phalloidin and nucleotide-binding sites on actin. *Eur. J. Biochem.*, 162(3):583–588, Februar 1987.
- [23] J.A. Theriot. The Polymerization Motor. *Traffic*, 1:19–28, 2000.
- [24] J.A. Theriot and T.J. Mitchison. Actin microfilament dynamics in locomoting cells. *Nature*, 352:126–131, 1991.

- [25] P.A. Janmey. The Cytoskeleton and Cell Signaling: Component Localization and Mechanical Coupling. *Physiol. Rev.*, 78(3):763–781, July 1998.
- [26] J.V. Small, M. Herzog, and K. Anderson. Actin filament organization in the fish keratocyte lamellipodium. *J. Cell Biol.*, 129:1275–1286, 1995.
- [27] K.I. Anderson and R. Cross. Contact dynamics during keratocyte motility. *Current Biology*, 10:253–260, 2000.
- [28] K.I. Anderson, Y.-L. Wang, and J.V. Small. Coordination of protrusion and translocation of the keratocyte involves rolling of the cell body. *J. Cell Biol.*, 134:1209–1218, 1996.
- [29] M. Doi, S.F. Edwards. *The Theory of Polymer Dynamics*. Oxford University Press, 2001.
- [30] M.B. Huglin. *Light Scattering from Polymer Solutions*. Academic Press, 1972.
- [31] M.H. Symons and T.J. Mitchison. Control of actin polymerization in live and permeabilized fibroblasts. *J. Cell Biol.*, 114:503–513, 1991.
- [32] M.O. Steinmetz, D. Stoffer, and A. Hoenger. Actin: From Cell Biology to Atomic Detail. *Journal of Structural Biology*, 119:295–320, 1997.
- [33] N. Suzuki, Y. Tamura, K. Mihashi. Compressibility and specific volume of actin decrease upon G to F transformation. *Biochemica et Biophysica Acta*, 1292:265–272, 1996.
- [34] Omega Optical incorporated.
<http://www.omegafilters/curvomatic/spectra.php>.
- [35] P. Kratochvil. *Classical Light Scattering from Polymer Solutions*. Elsevier, 1987.
- [36] P.A. Janmey, J.X. Tang, and C.F. Schmidt. Actin Filaments.
http://expmed.bwh.harvard.edu/projects/polymer/actin_chapter/.

- [37] P.S. Niranjana, J.G. Forbes, S.C. Greer, J. Dudowicz, K.F. Freed, J.F. Douglas. Thermodynamic regulation of actin polymerization. *Journal of Chemical Physics*, 114(24):10573–76, June 2001.
- [38] R. Rohrbach, E.H.K. Stelzer. Optical Trapping of dielectric particles in arbitrary fields. *J. Opt. Soc. Am. A*, 18(4):839–853, April 2001.
- [39] S.A. Aaronson and G.J. Todaro. Development of 3T3-like lines from Balb-c mouse embryo cultures: transformation susceptibility to SV40. *J. Cell. Physiol.*, 72:141–148, 1968.
- [40] S.R. Heidemann and R.E. Buxbaum. Cell Crawling: First the Motor, Now the Transmission. *The Journal of Cell Biology*, 141:1–4, 1998.
- [41] Stoffler.
<http://www.mih.unibas.ch/Homepages/stoffler/Slides/Actin/Actin.html>.
- [42] T. Dennerll, H. Joshi, V. Steel, R. Buxbaum, and S. Heidemann. Tension and compression in the cytoskeleton of PC-12 neurites. II: Quantitative measurements. *The Journal of Cell Biology*, 107:665–674, 1988.
- [43] T. Oliver, J. Lee, K. Jacobson. Forces exerted by locomoting cells. *Sem. Cell Biol.*, 5:139–147, 1994.
- [44] T.D. Pollard, and J.A. Cooper. Actin and Actin-Binding Proteins. A Critical Evaluation of Mechanisms and Functions. *Annu. Rev. Biochem.*, 55:987–1035, 1986.
- [45] T.J. Mitchison. Compare and Contrast Actin Filaments and Microtubules. *Molecular Biology of the Cell*, 3:1309–1315, 1992.
- [46] T.J. Mitchison and L.P. Cramer. Actin-Based Cell Motility and Cell Locomotion. *Cell*, 84:371–379, 1996.
- [47] T.J. Pollard. Rate Constants of ATP- and ADP-Actin with the Ends of Actin Filaments. *The Journal of Cell Biology*, 103:2747–54, 1986.

- [48] T.M. Svitkina, A.B. Verkhovsky, K.M. McQuade, and G.G. Borisy. Analysis of the Actin-Myosin II System in Fish Epidermal Keratocytes: Mechanism of Cell Body Translocation. *The Journal of Cell Biology*, 139:397–415, 1997.
- [49] T.P. Stossel. On the Crawling of Animal Cells. *Science*, 260:1086–1094, 1993.
- [50] Y. Harada, A. Toshimitsu. Radiation forces on a dielectric sphere in the Rayleigh scattering regime. *Optics Communications*, 124:529–541, 1996.

Vita

Michael Gögler was born in Füssen, Germany on August 24, 1977, the son of Rita Katharina Gögler and Lorenz Gögler. He received his Abitur at the Gymnasium Hohenschwangau in 1996. The next thirteen months he spent in mandatory civil service. The following year he was employed as a pflegerische Hilfskraft at the Fachklinik Enzensberg. He entered the Bayerische Julius Maximilians Universität Würzburg, Germany, as a physics student in 1998 where he received his Vordiplom two years later. After studying physics one more year in Würzburg he entered the graduate school at The University of Texas at Austin in Fall of 2001. He was supported by a partial scholarship of the Deutscher Akademischer Austausch Dienst. Additionally, he received BAföG from the Ministerium für Bildung und Forschung.

Permanent address: Ritterstraße 6
87629 Füssen
Germany

This thesis was typeset with L^AT_EX[†] by the author.

[†]L^AT_EX is a document preparation system developed by Leslie Lamport as a special version of Donald Knuth's T_EX Program.